Preprints.org

Article

Not peer-reviewed version

Symmetry in Nuclear Physics and Astrophysics

Jelena Vesic *

Posted Date: 19 January 2026

doi: 10.20944/preprints202601.1421.v1

Keywords: nuclear symmetry; isospin; symmetry energy; neutron stars; equation of state; heavy-ion collisions; charge-exchange reactions; electric dipole moments; neutrinoless double-beta decay

Preprints.org is a free multidisciplinary platform providing preprint service that is dedicated to making early versions of research outputs permanently available and citable. Preprints posted at Preprints.org appear in Web of Science, Crossref, Google Scholar, Scilit, Europe PMC.

Copyright: This open access article is published under a Creative Commons CC BY 4.0 license, which permit the free download, distribution, and reuse, provided that the author and preprint are cited in any reuse.

Preprints.org (www.preprints.org) | NOT PEER-REVIEWED | Posted: 19 January 2026 doi:10.20944/preprints202601.1421.v1

Disclaimer/Publisher's Note: The statements, opinions, and data contained in all publications are solely those of the individual author(s) and contributor(s) and not of MDPI and/or the editor(s). MDPI and/or the editor(s) disclaim responsibility for any injury to people or property resulting from any ideas, methods, instructions, or products referred to in the content.

Article

Symmetry in Nuclear Physics and Astrophysics

Jelena Vesic

Jožef Stefan Institute, Jamova cesta 39, Ljubljana, Slovenia
* Correspondence: jelena.vesic@ijs.si

Abstract

Symmetry is a key principle in physics that links basic invariances to the structure of matter and the evolution of the universe. In this review, we use symmetry as a unifying thread connecting nuclear structure, nuclear reactions, and dense matter, and we highlight how symmetry-based arguments connect laboratory observables to astrophysical constraints. We present the essential concepts in a form accessible to a broad physics audience.

Keywords: nuclear symmetry; isospin; symmetry energy; neutron stars; equation of state; heavy-ion collisions; charge-exchange reactions; electric dipole moments; neutrinoless double-beta decay

1. Introduction

Symmetry offers a compact way to formulate the laws of nature and helps explain why systems that differ widely in scale can behave similarly. Nuclei provide a rich testing ground. They are composed of protons and neutrons that interact primarily through the strong interaction, with electromagnetic and weak interactions playing important roles in nuclear structure, stability, and decay. They show a wide range of regularities and patterns. The link between symmetry and conservation laws is described by Noether's theorem, which states that every continuous symmetry of the action corresponds to a conserved quantity. Time-translation symmetry implies conservation of energy; space-translation symmetry implies conservation of linear momentum; and rotational symmetry implies conservation of angular momentum [1]. These invariances are built into essentially all descriptions of nuclear structure and reactions. Discrete symmetries such as parity (P), charge conjugation (C), and time reversal (T) play a fundamental role [50]. Violations of these symmetries test the Standard Model. Parity violation in weak interactions was first proposed by Lee and Yang and then confirmed experimentally by Wu et al. [46,47]. CP violation has also been observed in weak-interaction processes [50]. The CP violation present in the Standard Model appears insufficient to account for the observed matter–antimatter asymmetry of the universe, motivating ongoing searches for additional sources of CP violation [2,44,45]. Searches for permanent electric dipole moments provide particularly sensitive probes of such CP-violating physics within and beyond the Standard Model [3,4]. Beyond these fundamental invariances, nuclear physics is shaped by approximate symmetries that reflect properties of the nuclear force. Isospin symmetry, an approximate SU(2) invariance, treats protons and neutrons as two states of a single nucleon with respect to the strong interaction [5,6]. Although it is broken by the Coulomb force and by small charge-dependent components of the nuclear interaction, isospin remains a key organizing principle [7,8]. In the strong-interaction limit, it underlies mirror symmetry and the systematics of isobaric analogue states [8,56,133]. At the many-body level, collective symmetries such as SU(3) and $\mathrm{Sp}(3,\mathbb{R})$ emerge from correlated many-nucleon motion and enable compact descriptions of rotational and vibrational behavior in light and medium-mass nuclei [12–15]. Collective excitations such as giant resonances provide complementary, symmetry-sensitive benchmarks for nuclear dynamics [58,59]. Mixed-symmetry states, identified through characteristic M1 and E2 transition strengths, reveal the interplay of proton and neutron quadrupole collectivity [16,42]. Additional symmetry concepts, including pseudospin and F-spin, further clarify systematic patterns

© 2025 by the author(s). Distributed under a Creative Commons CC BY license.

Preprints.org (www.preprints.org) | NOT PEER-REVIEWED | Posted: 19 January 2026 doi:10.20944/preprints202601.1421.v1

across isotopic chains [17,18,67]. Qualitatively, these patterns suggest a familiar picture: the nucleus behaves like a quantum droplet. When many nucleons move coherently, a few collective degrees of freedom, such as quadrupole deformation and pairing correlations, often shape what we observe. Similar level schemes can arise from different underlying mechanisms (e.g., static deformation, configuration mixing in the shell model, or shape coexistence). A particularly important bridge between nuclear physics and astrophysics is the nuclear symmetry energy $S(n)$. It quantifies the leading (quadratic) energy cost of isospin asymmetry in nuclear matter at baryon density n and constitutes the isovector component of the nuclear equation of state (EoS). We adopt the standard notation [22,134]:

$$J = S(n_s), \qquad L = 3n_s \left.\frac{dS}{dn}\right|_{n=n_s}, \qquad K_{\rm sym} = 9n_s^2 \left.\frac{d^2S}{dn^2}\right|_{n=n_s}. \tag{1}$$

Here n_s denotes the saturation density of symmetric nuclear matter (often denoted as n_0), $n_s \simeq 0.16\ \mathrm{fm}^{-3}$. Near saturation density, J is relatively well constrained, whereas L remains less tightly constrained by laboratory and theoretical analyses; the inferred ranges depend on the adopted models, observables, and statistical methodology [19–22,24,25,31]. Many quoted constraints are conditional on framework-specific correlations (e.g., within a given energy-density functional (EDF) family, within chiral effective field theory (EFT) extrapolations beyond the fitted domain, or under specific Bayesian prior choices). Accordingly, cross-study comparisons should report both statistical uncertainties and framework-dependent systematics tied to modeling assumptions and calibration data. At supra-saturation densities, the density dependence of the symmetry energy contributes to the pressure of neutron-rich matter and influences neutron-star radii, tidal deformabilities, and crust properties, while affecting the maximum mass more indirectly [25–27,32]. The maximum mass is primarily set by the high-density stiffness of the EoS. Gravitational-wave observations beginning with GW170817 [28] and subsequent GW170817-based EoS analyses, together with NICER (Neutron star Interior Composition Explorer) pulse-profile modeling of individual millisecond pulsars, indicate radii of order 11–13 km [29,30,144]. The growing overlap between constraints from laboratory experiments and astrophysical observations shows why symmetry-based descriptions are useful. They provide a shared framework for comparing results across scales. Experimental progress has also been significant. Rare-isotope facilities such as FRIB (Facility for Rare Isotope Beams), RIBF (Radioactive Isotope Beam Factory), GSI/FAIR (GSI Helmholtz Centre for Heavy Ion Research/Facility for Antiproton and Ion Research), and GANIL/SPIRAL2 (Grand Accélérateur National d'Ions Lourds/Système de Production d'Ions Radioactifs Accélérés en Ligne 2) increasingly probe nuclei at extreme neutron–proton asymmetry, where weak binding and coupling to the particle continuum can enhance sensitivity to symmetry-related effects. High-resolution charge-exchange reactions, especially modern $(^3\mathrm{He}, t)$ measurements, map Gamow–Teller (GT) strength distributions with energy resolutions as good as 30–40 keV in favorable cases [33–36]. While these advances enhance the experimental input, quantitative symmetry constraints still depend on reaction modeling, the treatment of the continuum and correlations, and (for some observables) on reliably disentangling competing multipoles. Additional information comes from β-decay studies of exotic nuclei, including measurements on highly charged ions, which provide complementary constraints on spin–isospin response and isospin-symmetry systematics [39]. Parity-violating electron scattering, discussed in detail below, provides an independent probe of neutron distributions and isovector structure [23]. Finally, precision mass spectrometry, laser spectroscopy, and modern γ-ray spectroscopy and tracking arrays provide inputs such as masses, charge radii, electromagnetic moments, and transition strengths that underpin quantitative studies of isospin symmetry, its breaking, and the density dependence of the symmetry energy [37,38,40,41]. In this review, we show how symmetry arguments organize complex nuclear many-body dynamics and connect laboratory observables to astrophysical phenomena. We present the key symmetry concepts in a form accessible to non-specialists.

© 2025 by the author(s). Distributed under a Creative Commons CC BY license.

Preprints.org (www.preprints.org) | NOT PEER-REVIEWED | Posted: 19 January 2026 doi:10.20944/preprints202601.1421.v1

2. Types of Symmetries in Nuclear Physics

In nuclear physics, symmetry appears in several different forms. At the most basic level, it refers to properties that remain unchanged under specific transformations, such as rotations, translations in space or time, or the (approximate) exchange of protons and neutrons. This leads to a hierarchy of symmetry concepts. These include exact space-time invariances and discrete symmetries of the underlying Hamiltonian, approximate internal symmetries such as isospin and chiral symmetry [43], emergent collective symmetries associated with rotational and vibrational motion, more specialized symmetries, including pseudospin and F-spin, and, finally, situations in which symmetries are broken at the mean-field level and restored through quantum correlations. These symmetries, and the mechanisms that break them, shape nuclear structure, nuclear reaction dynamics, and the behavior of dense astrophysical matter. Their study constrains nuclear interaction and many-body correlations, and it also sets the stage for the discussion of the symmetry energy and astrophysical phenomena in later sections. We will group nuclear symmetries into six broad, interconnected classes: fundamental space–time symmetries; collective and group-theoretical symmetries; isospin and related charge symmetries; specialized or "exotic" symmetries that emerge in particular regions of the nuclear chart; chiral and QCD-inspired symmetries; and symmetry breaking and restoration. Each class contributes in a distinct way to the phenomenology of finite nuclei and infinite nuclear matter, but together they highlight the unifying role of symmetry concepts in nuclear physics. The discrete symmetries P (parity) and T (time reversal), as well as their combinations with charge conjugation (C), further connect nuclear physics to particle physics and cosmology and provide some of the most sensitive low-energy probes of physics beyond the Standard Model [2–4]. Table 1 summarizes this classification and highlights representative symmetry concepts, their physical origins, and a few key observables.

2.1. Fundamental Space-Time Symmetries

Space–time symmetries describe invariance under time translations, spatial translations, and rotations. These continuous symmetries underlie the familiar conservation laws of energy, linear momentum, and angular momentum [1] and are among the most robust principles in physics. Discrete symmetries such as parity (P), charge conjugation (C), and time reversal (T) are more subtle. In relativistic quantum field theory, CPT invariance is expected on very general grounds [48,49]. High-precision tests of CP, T, and CPT symmetries provide especially sensitive low-energy probes for physics beyond the Standard Model [2–4,50].

2.2. Collective Symmetries

Collective symmetries emerge from correlated many-nucleon dynamics and offer compact descriptions of rotational and vibrational modes in light and medium-mass nuclei. A classic example is the (approximate) Elliott SU(3) symmetry of the harmonic-oscillator shell model, which organizes quadrupole collectivity and rotational-band structures. Although spin–orbit splittings and other non-harmonic terms break this symmetry in real nuclei, it often remains a useful organizing scheme [12–15]. Symplectic extensions such as $\mathrm{Sp}(3,\mathbb{R})$ constitute a framework for large-amplitude collective motion, multi-$\hbar\omega$ correlations, and deformation within a microscopic many-body description [14,15]. Collective excitations such as giant resonances serve as benchmarks of nuclear response and effective interactions in both the isoscalar and isovector channels [58,59].

2.3. Isospin Symmetry and Charge Symmetry

Isospin symmetry, introduced by Heisenberg and Wigner, treats protons and neutrons as two quantum states (often described as projections) of a single nucleon, forming an isospin doublet [5,6]. If this symmetry were exact for the strong interaction (i.e., neglecting electromagnetic effects and other isospin nonconserving terms), nuclear interactions would be charge independent, and mirror nuclei would be identical in the strong-interaction limit. Coulomb shifts break this degeneracy [7]. Isobaric analogue states in different nuclei with the same mass number and total isospin would be degenerate in the strong-interaction limit. Isospin symmetry is only approximate, but it captures essential features

© 2025 by the author(s). Distributed under a Creative Commons CC BY license.

Preprints.org (www.preprints.org) | NOT PEER-REVIEWED | Posted: 19 January 2026 doi:10.20944/preprints202601.1421.v1

of the nuclear force and allows controlled deviations from it to be quantified. Accordingly, it provides a sensitive probe of Coulomb effects and charge-dependent components of the strong interaction [7,53]. Two related invariances commonly used to classify isospin-breaking effects are charge independence and charge symmetry. Charge independence refers to invariance under arbitrary rotations in isospin space, whereas charge symmetry refers specifically to invariance under a 180° rotation that exchanges protons and neutrons [7]. Charge-symmetry-breaking and charge-independence-breaking effects are observed in scattering-length differences, mirror energy shifts, non-degenerate isobaric analogue states, and mirror asymmetries in β decay [7,8,51]. High-precision mass measurements and systematics of isobaric analogue states provide quantitative constraints on these effects [56], and they serve as benchmarks for modern chiral effective field-theory interactions and energy-density functionals [43,57]. Coulomb repulsion among protons breaks isospin symmetry and generates measurable phenomena such as mirror displacement energies, Thomas–Ehrman shifts in weakly bound nuclei, and enhanced isospin mixing near the proton drip line [8,52–55]. Experiments on proton-rich exotic nuclei reveal pronounced asymmetries in decay and transition strengths close to the drip line, where small separation energies enhance sensitivity to Coulomb effects and coupling to the continuum [103]. β-decay spectroscopy of ^{27}S provides a representative recent experimental example [51]. Mirror nuclei serve as probes of the charge-dependent nuclear interaction [7,52]. A particularly sensitive class of observables is provided by mirror energy differences (MED) between analogue states in $T = 1/2$ nuclei. A systematic shell-model analysis of MED in the $A = 42$–54 region has been used to constrain effective isovector interactions $(V_{pp} - V_{nn})$ that include both Coulomb and nuclear charge-dependent terms [8,52]. The results indicate that Coulomb effects alone do not reproduce the full MED systematics and that additional isospin-nonconserving nuclear contributions are required in effective Hamiltonians [52]. Such studies therefore place constraints on charge-symmetry-breaking and charge-independence-breaking terms in modern shell-model descriptions.

2.4. Pseudospin, F-Spin, and Other Specialized Symmetries

Some nuclear symmetries are more abstract and can be viewed as regularities in the single-particle spectrum or in patterns of collective states. Pseudospin and F-spin are examples of such "internal" symmetries: pseudospin helps organize single-particle levels into near-degenerate doublets [65,66], while F-spin provides a useful classification of proton–neutron degrees of freedom in collective models [18,67]. These ideas are particularly useful in heavy nuclei and along isotopic chains, where regularities emerge despite complex spectra. In relativistic mean-field language, pseudospin symmetry emerges as an approximate symmetry when the sum of the Dirac scalar and vector mean fields, $\Sigma(r) \equiv V_S(r) + V_V(r)$, varies slowly (i.e., $d\Sigma/dr \approx 0$), which corresponds to the pseudospin-symmetric limit and reflects an underlying SU(2) symmetry of the Dirac Hamiltonian [65,66]. This pseudospin perspective clarifies the relativistic origin of shell structure and its evolution toward weakly bound systems. Furthermore, F-spin symmetry within the proton–neutron interacting boson model (IBM-2) [18,67] provides a systematic way to classify proton and neutron bosons, in which the F-spin quantum number F quantifies proton–neutron mixing. Mixed-symmetry states, typically associated with the F-spin sector $F = F_{\max} - 1$ in the IBM-2 classification, serve as sensitive probes of proton–neutron correlations and of the evolution of collective behavior along isotopic chains (see, e.g., [16,68]). Near the drip lines, where nuclear binding is weak, halo nuclei such as ^{11}Li and ^{6}He display extended matter distributions, altered pairing correlations due to continuum coupling, and enhanced low-energy electric dipole (E1) strength [70]. Cluster configurations, including α clustering in ^{12}C and ^{16}O, reveal emergent spatial symmetries and are effectively modeled using algebraic and microscopic cluster theories [69]. Shape coexistence, defined by the presence of multiple nuclear shapes at comparable energies, indicates the existence of competing local minima in the nuclear energy landscape and can be analyzed through configuration mixing and mean-field-based studies [71]. Unconventional pairing correlations are expected to be most pronounced in $N \approx Z$ nuclei in the mass $A \approx 90$–100 region, where neutrons and protons occupy the same high-j orbitals and isovector ($T = 1$) and isoscalar ($T = 0$) correlations may compete [72]. Evidence consistent with a spin-aligned $T = 0$

© 2025 by the author(s). Distributed under a Creative Commons CC BY license.

Preprints.org (www.preprints.org) | NOT PEER-REVIEWED | Posted: 19 January 2026 doi:10.20944/preprints202601.1421.v1

pairing phase has been reported in the $N = Z = 46$ nucleus ^{92}Pd, where the yrast level pattern was interpreted in terms of spin-aligned neutron–proton (np) pairs [73]. This behavior differs from the level schemes of neighbouring nuclei and suggests that approximate symmetries in the pairing channel may evolve qualitatively toward the $N = Z$ line. Pairing correlations can also be discussed in terms of an approximate seniority symmetry, which classifies states by the number of unpaired nucleons and explains level systematics near shell closures [74].

2.5. Chiral Symmetry and QCD-Inspired Symmetries

At the most fundamental level, nuclear structure and interactions emerge from quantum chromodynamics (QCD) [79]. While QCD cannot yet be solved routinely for complex nuclei, its approximate chiral symmetry provides the symmetry basis for constructing the low-energy nuclear force within effective field theory [43,75–77]. The spontaneous breaking of chiral symmetry in the QCD vacuum gives rise to pions as pseudo-Goldstone bosons; consequently, pion exchange dominates the long-range part of the nuclear interaction and provides a leading contribution to its characteristic spin–isospin dependence [43,77]. Chiral effective field theory (chiral EFT) incorporates these QCD symmetries and provides a systematic expansion of nuclear forces, including consistent many-body interactions, together with a systematic framework for estimating truncation uncertainties [43,77,79]. Quantitative predictions and uncertainty budgets remain sensitive to regulator choices, the calibration of low-energy constants (LECs), and assumptions about the breakdown scale of the expansion [77,79]. Within this framework, pion exchange and associated two-body axial currents provide important contributions to GT transitions, β decay, and neutrino–nucleus scattering [78,79]. Recent *ab initio* calculations based on chiral EFT interactions have clarified links between the properties of finite nuclei, neutron matter, and the nuclear symmetry energy, enabling constraints to be propagated with model-dependent extrapolations in density to astrophysical observables such as neutron-star radii and tidal deformabilities [20,21].

2.6. Symmetry Breaking and Restoration in Nuclei

Mean-field descriptions of nuclei often involve intrinsic states that break symmetries of the underlying Hamiltonian [80]. Typical examples include the breaking of rotational symmetry in deformed nuclei and particle-number symmetry in pairing condensates, as well as explicit isospin breaking by the Coulomb interaction. This intrinsic (spontaneous) symmetry breaking is not an exact property of the physical system; rather, it reflects an efficient approximation to the correlated many-body state. Equivalently, broken-symmetry intrinsic states are convenient reference states. Good quantum numbers are recovered once correlations are incorporated through symmetry restoration (projection) and, where necessary, configuration mixing. Typically, symmetry restoration is implemented by combining projection techniques with configuration mixing frameworks such as the generator-coordinate method (GCM) [80]. Angular-momentum projection yields states with good rotational quantum numbers and generates rotational band structures, while particle-number projection improves the description of pairing correlations. Collective symplectic structures may re-emerge even when SU(3)-like symmetries are strongly broken at the single-particle level [14,15]. The interplay between symmetry breaking and restoration provides a measure of many-body correlations and is needed for reliable descriptions of spectra and transition strengths.

© 2025 by the author(s). Distributed under a Creative Commons CC BY license.

Preprints.org (www.preprints.org) | NOT PEER-REVIEWED | Posted: 19 January 2026 doi:10.20944/preprints202601.1421.v1

Table 1. Classes of symmetries in nuclear physics and their physical roles (illustrative).

Symmetry Class	Representative Symmetries	Physical Origin and Description	Key Phenomena and Observables
Fundamental space–time and discrete symmetries	Time translations; spatial translations; rotations; discrete C, P, T (and combinations such as CP, CPT)	Exact invariances associated with space–time structure for an isolated system; discrete-symmetry conservation/violation depends on the interaction (with CPT invariance ensured in local Lorentz-invariant QFT under standard assumptions)	Conservation of energy, momentum, and angular momentum; parity- and time-reversal-violation tests (e.g., EDMs, parity-violating observables)
Isospin and charge symmetries	SU(2) isospin; charge independence; charge symmetry ($p \leftrightarrow n$)	Approximate internal symmetry of the strong interaction treating protons and neutrons as an isospin doublet; broken by Coulomb and charge-symmetry/charge-independence breaking terms	Isobaric analogue states (IAS); charge-exchange reactions; superallowed and allowed β decay; IMME systematics; probes of isospin breaking (MED, isospin mixing)
Collective and group-theoretical symmetries	SU(3); $\mathrm{Sp}(3,\mathbb{R})$	Emergent (often approximate) symmetries arising from correlated many-body motion	Rotational bands; vibrational spectra; collective modes (including giant resonances); quadrupole collectivity
Specialized symmetries	Pseudospin; F-spin; clustering symmetries; seniority/pairing	Approximate or emergent regularities in specific regions of the nuclear chart and/or within restricted model spaces	Near-degenerate single-particle doublets; mixed-symmetry states; seniority systematics and pairing gaps; isoscalar $T = 0$ pairing
Chiral and QCD-inspired symmetries	Approximate chiral symmetry; chiral EFT expansion	Approximate chiral symmetry of QCD and its spontaneous breaking; basis for low-energy nuclear forces and currents	Long-range pion exchange; consistent nuclear forces and electroweak currents; uncertainty quantification in chiral EFT
Symmetry breaking and restoration	Mean-field breaking of rotational symmetry and particle-number global $U(1)$ symmetry; explicit isospin breaking (Coulomb)	Efficient approximations that break symmetries at the mean-field level, restored by quantum correlations (projection, configuration mixing)	Deformation; pairing condensates; projection methods; configuration mixing; restoration of good quantum numbers; shape coexistence

With this taxonomy in place, we now summarize the experimental methodologies that most directly access these symmetry concepts and their breaking mechanisms.

3. Experimental Methodologies and Technical Capabilities

Nuclear symmetry studies depend on a broad suite of experimental approaches, each of which highlights different aspects of nuclear structure, dynamics, and interactions in systems with neutron–proton asymmetry. No single observable determines all symmetry properties. Instead, constraints are obtained by combining complementary measurements, quantifying theoretical and experimental

© 2025 by the author(s). Distributed under a Creative Commons CC BY license.

Preprints.org (www.preprints.org) | NOT PEER-REVIEWED | Posted: 19 January 2026 doi:10.20944/preprints202601.1421.v1

uncertainties, and exploiting advances in detector development and accelerator technology. In this section, we outline the main experimental methods used to probe the symmetry concepts introduced in Section 2 and emphasize the observables they constrain and the dominant limitations. For each method, we highlight specific symmetry aspects, such as the density dependence of the symmetry energy, isospin-symmetry breaking, or the spin–isospin response, and we indicate how laboratory observables can be connected, directly or indirectly, to neutron-star and supernova physics [24,33,81,82,84].

3.1. Heavy-Ion Collisions and the Symmetry Energy

Heavy-ion collisions probe the symmetry energy over a broad range of densities and temperatures, but quantitative constraints depend on transport-model descriptions and their associated systematics [81,82,85]. The symmetry energy acts as an isovector "pressure" that drives neutron–proton separation, equilibration, and emission [81,82]. At near-Fermi energies (roughly 30–100 MeV per nucleon), collisions undergo compression–expansion dynamics that primarily sample sub-saturation to near-saturation densities [81,82]. Key observables include isospin diffusion, isoscaling parameters extracted from fragment yields [141], and neutron-to-proton spectral ratios, reflecting both mean-field dynamics and transport properties [81–83]. Symmetry-energy information is inferred by comparison with transport calculations rather than extracted directly from a single observable. Within transport-model analyses, the inferred degree of isospin equilibration can decrease for a stiffer symmetry energy, enabling constraints on the slope parameter L when combined with systematic uncertainty estimates [24,83,86]. A central limitation is parameter degeneracy: similar trends can arise from the isovector mean field, in-medium cross sections, cluster production, and event selection, and the inferred symmetry-energy sensitivity can vary across transport implementations [96,139]. At higher beam energies (roughly 400 MeV$/A$ to several GeV$/A$), experiments access supra-saturation densities using meson and photon observables, most prominently pion and kaon production ratios [87,88]. Ratios such as π^-/π^+ increase with neutron excess and, in some transport-model implementations, have been linked to a softer symmetry energy at high density, although the interpretation remains strongly model dependent [87,140]. The inferred high-density behavior shifts when Δ dynamics, pion production/absorption, and meson potentials are treated differently. Accordingly, pion-based constraints are conditional on the transport implementation [139,140]. Kaon ratios (K^0/K^+) have been proposed as complementary probes that can be less sensitive to some late-stage hadronic effects in certain regimes [89]. Hard photons from neutron–proton bremsstrahlung are emitted mainly in the early, pre-equilibrium stage and, because they have comparatively little final-state interaction, provide a penetrating probe of the reaction dynamics [90]. Quantitative inferences at supra-saturation density can vary significantly across transport implementations due to differences in mean fields, cluster production, in-medium cross sections, and meson potentials. Results should be reported with explicit code dependence and prior sensitivity supported by inter-code benchmarks [96]. Key experimental efforts include the ASY-EoS campaign at GSI [91] and large-acceptance spectrometer systems such as SAMURAI (Superconducting Analyzer for MUlti-particles from RAdio Isotope beams) at the RIKEN Radioactive Isotope Beam Factory (RIBF) [92] and LAMPS (Large Acceptance Multi-Purpose Spectrometer) at RAON (Rare isotope Accelerator complex for ON-line experiments) [93], which combine high-granularity tracking with charged-particle and neutron detection to improve the interpretability of isospin-sensitive observables.

3.2. Charge-Exchange Reactions and Spin-Isospin Probes

Charge-exchange reactions, such as (p,n), (n,p), (d,^{2}He), and (^{3}He,t), provide a selective probe of the nuclear spin–isospin response. They induce charge-exchange transitions in the target nucleus, converting a neutron into a proton (or vice versa), and thus access transitions with $\Delta T_z = \pm 1$ (with $\Delta T = 0$ or 1) that are the nuclear analogues of weak processes. When measured at intermediate beam energies and very forward scattering angles (small momentum transfer), the response is dominated by $\Delta L = 0$ transitions, in particular Fermi ($\Delta S = 0$) and GT ($\Delta S = 1$) modes. Under $q \simeq 0$ conditions in the GT channel, the differential cross sections become approximately proportional to the GT transition

© 2025 by the author(s). Distributed under a Creative Commons CC BY license.

Preprints.org (www.preprints.org) | NOT PEER-REVIEWED | Posted: 19 January 2026 doi:10.20944/preprints202601.1421.v1

strength, once the unit cross section is calibrated [9–11]. A key challenge is that the proportionality is not universal: it degrades as the momentum transfer increases and can be affected by multistep processes, optical-model ambiguities, and interference with non-GT multipoles. Reliable strength extractions therefore require reaction modeling and internal consistency checks. The dominance of Fermi and GT components at very forward angles enables detailed mapping of GT strength distributions and studies of IAS, while measurements at finite angles and multipole-decomposition analyses provide access to higher-multipole spin–isospin excitations [33–36]. Modern experiments can achieve energy resolutions as good as 30–40 keV in favorable conditions, notably with dispersion-matched setups such as Grand Raiden at RCNP (Research Center for Nuclear Physics), Osaka University [94,98]. Other spectrometers, including K600 at iThemba LABS and the S800 spectrometer at NSCL (National Superconducting Cyclotron Laboratory)/FRIB, enable high-resolution charge-exchange studies with competitive performance depending on optics and detector configuration [95,97]. These capabilities allow GT strength to be traced up to excitation energies of order 20 MeV (nucleus-dependent), providing stringent tests of shell-model predictions and quantitative insight into configuration mixing and GT quenching mechanisms [10,33]. In an astrophysical context, GT transitions govern electron-capture and beta-decay rates in late stellar evolution and play a central role in neutrino–matter interactions in core-collapse supernovae [99]. Isobaric analogue states, accessed in the same charge-exchange reactions, constitute particularly clean probes of isospin symmetry and its breaking. Precise measurements of IAS excitation energies and strength distributions can help separate Coulomb contributions from charge-dependent components of the nuclear interaction and thus constrain isospin-symmetry-breaking and charge-independence-breaking terms in nuclear Hamiltonians, albeit with residual model dependence from reaction mechanisms and structure [8,35].

3.3. Beta Decay and Weak-Interaction Observables

Beta decay provides a complementary window on weak-interaction couplings, isospin structure, and symmetry breaking, particularly in nuclei close to the drip lines where weak binding and coupling to the continuum can reshape wave functions and transition strengths [102,103]. β decay probes the vector and axial-vector weak currents through Fermi (isospin) and GT (spin–isospin) operators, thereby constraining nuclear matrix elements that also enter astrophysical weak rates [99]. Precision tests additionally require radiative and isospin-symmetry-breaking corrections [100]. In-flight projectile fragmentation (or ISOL (isotope separation on-line) production) followed by implantation into highly segmented double-sided silicon strip detectors (DSSSDs) enables event-by-event correlations between implanted ions and their subsequent decays [101,104]. This approach supports the identification of very rare decay branches and the detection of low-energy charged particles, including β-delayed protons with energies down to the sub-MeV regime (and, in favorable cases, a few hundred keV), provided that thresholds, β summing, and correlation-window backgrounds are carefully accounted for [101,102]. Such sensitivity is especially crucial near the proton drip line, where small proton separation energies enhance Coulomb and continuum effects and mirror asymmetries in β decay can become pronounced; the β-decay spectroscopy of ^{27}S provides a representative example and attributes a large mirror asymmetry to weak-binding effects in the proton $1s_{1/2}$ orbit [51]. High-precision half-life and Q-value measurements, using Penning traps and dedicated decay stations (and, in selected cases, storage-ring techniques), are central to tests of the weak interaction and the unitarity of the Cabibbo–Kobayashi–Maskawa (CKM) matrix, most notably through the superallowed $0^+ \to 0^+$ program. They require systematic control of radiative and isospin-symmetry-breaking corrections [100]. β-delayed particle emission (protons, neutrons, α particles) provides access to unbound states and resonance properties in exotic nuclei and remains one of the most direct experimental routes to spectroscopy at and beyond the drip lines. The quantitative interpretations can depend on line-shape modeling, detector response, and feeding from unresolved states [102,103]. Beyond single-particle emission, multi-particle decay modes (e.g., $\beta 2p$, $2p$, and correlated emissions) probe nucleon–nucleon correlations in weakly bound systems. Recent developments in highly segmented implantation arrays

© 2025 by the author(s). Distributed under a Creative Commons CC BY license.

Preprints.org (www.preprints.org) | NOT PEER-REVIEWED | Posted: 19 January 2026 doi:10.20944/preprints202601.1421.v1

and tracking detectors improve reconstruction of complex decay topologies, but demand careful efficiency calibration and event-classification systematics [103,104].

3.4. Gamma-Ray Spectroscopy and Lifetime Measurements

Gamma-ray spectroscopy provides direct experimental access to nuclear level schemes and electromagnetic decay patterns, enabling structural systematics that frequently expose emergent symmetries (e.g., rotational and vibrational sequences) and their breaking. High-efficiency Compton-suppressed HPGe (high-purity germanium) arrays such as GAMMASPHERE [105] and INGA (Indian National Gamma Array) [40,106] provide high photopeak efficiency and excellent energy resolution, while tracking arrays such as AGATA (Advanced GAmma Tracking Array) [41] and the GRETINA (Gamma-Ray Energy Tracking In-beam Nuclear Array, as the first stage toward the full 4π GRETA (Gamma-Ray Energy Tracking Array) concept) [107,108] add interaction-position reconstruction for event-by-event Doppler correction and γ-ray tracking. The measured energies establish level spacings and band or multiplet structures. Intensities, angular distributions, and angular correlations determine branching ratios, multipolarities, and mixing ratios, enabling quantitative comparisons with collective and shell-model descriptions. Lifetime measurements (using DSAM (Doppler-shift attenuation method), recoil-distance/plunger methods, and fast-timing techniques) set the absolute scale of transition strengths through $B(EL)$ and $B(ML)$ values. The recoil-distance Doppler-shift (RDDS) method provides access to lifetimes and absolute transition probabilities in the $\sim 10^{-12}$–10^{-9} s range over a broad range of reactions and kinematics [109], while modern γ–γ fast timing with $LaBr_3$(Ce) extends sensitivity to very short lifetimes with well-characterized timing response functions [110]. These observables constrain electromagnetic matrix elements and help disentangle isoscalar and isovector components. For example, in the $A = 31$ mirror pair, selected $E1$ strengths exhibit a sizable induced isoscalar component (reported at the ∼24% level of the isovector contribution) [111]. Systematic studies of proton–neutron mixed-symmetry excitations in vibrational and transitional nuclei provide stringent constraints on proton–neutron quadrupole correlations and on the effective interactions used in collective models [16]. A main challenge is that precision electromagnetic matrix elements are often limited by systematic effects rather than statistics: efficiency and summing corrections, Doppler-reconstruction systematics (velocity distributions, stopping powers, and lineshape modeling), side-feeding and unresolved feeding, angular-correlation assumptions, and the treatment of background and contaminant lines. Robust conclusions about symmetry signatures usually require redundant observables (energies, branching ratios, mixing ratios, lifetimes) and cross-checks across reaction mechanisms and detector configurations [109,110].

3.5. Parity-Violating Electron Scattering

Parity-violating electron scattering (PVES) uses the weak neutral current as a probe of neutron distributions and related isovector properties relevant to the symmetry energy. The parity-violating asymmetry arises from γ–Z^0 interference [162,163]. The parity-violating asymmetry is defined as

$$A_{\mathrm{PV}} = \frac{\sigma_R - \sigma_L}{\sigma_R + \sigma_L}, \tag{2}$$

where $\sigma_{R(L)}$ denotes the differential cross section for right- (left-) handed electrons. The neutron weak charge is much larger in magnitude than the proton weak charge [50,164]. As a result, A_{PV} is primarily sensitive to the nuclear weak form factor and thus to the neutron density, with substantially reduced strong-interaction reaction-model dependence compared to hadronic probes [113–115]. Quantitative extractions require treatment of Coulomb distortions, electroweak radiative corrections, acceptance averaging, and backgrounds, which are among the dominant sources of systematic uncertainty [114,115]. PVES isolates the weak neutral-current response at fixed momentum transfer, constraining the weak-charge form factor [162,163]. Translating A_{PV} into a neutron radius or skin requires a nuclear-structure parameterization and quantified theory input. Helicity-correlated instrumental effects and electroweak radiative corrections often set the scale of systematic uncertainties, while the total uncertainty in

© 2025 by the author(s). Distributed under a Creative Commons CC BY license.

Preprints.org (www.preprints.org) | NOT PEER-REVIEWED | Posted: 19 January 2026 doi:10.20944/preprints202601.1421.v1

flagship measurements can remain statistics limited. Experiments such as PREX (Pb Radius Experiment) [113,115] and CREX (Ca Radius Experiment) [114] employ highly polarized electron beams, precision magnetic spectrometers, dedicated Cherenkov detectors, and ultra-stable helicity control and beam monitoring to measure extremely small asymmetries. For elastic scattering at PREX/CREX kinematics, the asymmetries are typically at the sub-ppm to a few ppm scale (i.e., $\mathcal{O}(10^2\text{–}10^3)$ ppb), e.g., $A_{\rm PV} \approx 5.5 \times 10^2$ ppb for ^{208}Pb and $A_{\rm PV} \approx 2.668 \times 10^3$ ppb for ^{48}Ca depending on the kinematics [113,114]. Related parity-violation measurements on the proton (Qweak) probe the weak charge of the proton at comparably small asymmetries [112]. PVES enables the extraction of neutron radii and neutron-skin thicknesses with reduced strong-interaction model dependence via correlations within nuclear energy-density functionals. These measurements provide indirect constraints on the density dependence of the symmetry energy, commonly parameterized by the slope L [22]. PREX-II indicates a comparatively large neutron skin in ^{208}Pb [113], while CREX favours a smaller neutron skin in ^{48}Ca [114]. Achieving a consistent description across nuclei and momentum transfers has therefore become a key benchmark for EDF developments and uncertainty-quantified inferences [22,116]. The mapping from neutron-skin data to L is correlation driven and therefore conditional on the assumed EDF family and calibration strategy. PVES most directly constrains the weak form factor at the measured q, while the symmetry-energy inference adds a model-dependent step.

3.6. Radioactive Ion Beams and Exotic Nuclei

Radioactive ion beam (RIB) facilities such as RIKEN, GSI/FAIR, FRIB, ISOLDE (Isotope Separator On Line DEvice) at CERN, and SPIRAL2 enable systematic studies of nuclei far from stability, where weak binding, continuum coupling, and isospin asymmetry amplify symmetry breaking and emergent collective patterns. RIBs provide access to nuclei with extreme N/Z, allowing tests of nuclear interactions and many-body approximations in regimes that are inaccessible with stable beams. In-flight fragmentation and separation offer broad isotope coverage at intermediate and high energies, while ISOL techniques can deliver beams of high purity and excellent beam quality for precision experiments. Precision masses and selected spectroscopic observables can be extended to very short-lived nuclides using storage-ring techniques (including isochronous and Schottky mass spectrometry), reaching lifetimes from the tens-of-μs to ms regime in favorable conditions, depending on the mode and nuclei [117–119,128,129]. RIB experiments probe halo and skin phenomena, shell evolution, and isospin mixing in weakly bound systems through different reaction mechanisms. Coulomb excitation in inverse kinematics provides access to $E2$ and $E3$ matrix elements and hence to deformation, shape coexistence, and proton–neutron collectivity, including mixed-symmetry quadrupole modes [16,120,121]. Knockout, breakup, and charge-changing reactions, analyzed with eikonal/Glauber-based and continuum-sensitive descriptions, provide spectroscopic information and can constrain neutron-skin trends and symmetry-energy-related systematics when combined with theory [84,120]. Invariant-mass spectroscopy of unbound states in neutron-rich nuclei relies on large-acceptance spectrometers and high-efficiency neutron time-of-flight (ToF) arrays. Representative systems include LAND (Large Area Neutron Detector) at GSI and large-acceptance spectrometers SAMURAI at RIKEN, as well as MoNA–LISA (Modular Neutron Array–Large multi-Institutional Scintillator Array) at NSCL/FRIB for multi-neutron detection [122–125]. Here, the dominant experimental uncertainties are cross talk, efficiency calibration, and acceptance effects. On the theory side, continuum dynamics and final-state interactions can dominate the extracted resonance properties. Results should therefore be reported together with clearly stated reconstruction procedures, efficiency and cross-talk corrections, and sensitivity studies to the adopted reaction and continuum models [125].

3.7. Precision Mass Measurements and Isospin Structure

Nuclear masses encode binding energies and their finite differences (separation energies and Q values), and therefore provide direct, weakly model-dependent references for isospin systematics and for astrophysical reaction networks [37,126]. Penning-trap facilities such as ISOLTRAP (ISOLDE TRAP), TRIGA-TRAP (Training, Research, Isotopes, General Atomics TRAP), SHIPTRAP (Separator

© 2025 by the author(s). Distributed under a Creative Commons CC BY license.

Preprints.org (www.preprints.org) | NOT PEER-REVIEWED | Posted: 19 January 2026 doi:10.20944/preprints202601.1421.v1

for Heavy Ion reaction Products TRAP), TITAN (TRIUMF's Ion Trap for Atomic and Nuclear science), LEBIT (Low Energy Beam and Ion Trap), and JYFLTRAP (Jyväskylä TRAP) can achieve relative mass uncertainties down to the 10^{-9}–10^{-8} range in favorable cases, while precision for the shortest-lived species is typically limited by cycle time, isomeric contamination, and count-rate systematics [37,127]. These data support Coulomb displacement energies, enable stringent tests of the isobaric multiplet mass equation (IMME), and quantify isospin-symmetry-breaking contributions that must be controlled in precision weak-interaction studies and in global modeling [126]. Storage-ring techniques (isochronous and Schottky mass spectrometry) extend precision mass access to nuclides with very short lifetimes, reaching lifetimes from the tens-of-μs to ms regime in favorable conditions, depending on the mode and nuclei [117,128,129]. Because the ions are stored and repeatedly observed, storage rings provide access to both masses and decay properties in the same experimental environment, but this advantage comes with calibration-dominated uncertainties. Storage-ring mass extraction is intrinsically calibration-driven: magnetic-rigidity drifts, non-isochronicity corrections, charge-state ambiguities, and acceptance effects must be accounted for [128,129]. In astrophysics, such masses provide key inputs to *r*-process modeling and to neutron-star crust composition calculations, and they also benchmark global mass models used in broader symmetry-energy systematics [117,126].

3.8. Experimental Limitations and Systematic Uncertainties

Despite substantial experimental progress, studies of nuclear symmetries and symmetry breaking remain constrained by both instrumental effects and interpretative (model-mapping) ambiguities. Improved detector segmentation, fast digital signal processing, and high-granularity tracking have improved particle identification and background rejection. Active-target time-projection chambers (TPCs) and related target and vertexing concepts extend sensitivity to low-energy recoils and weakly bound systems by combining large acceptance with low thresholds, but they introduce their own challenges (field non-uniformities, space-charge distortions, gain stability, and efficiency calibration) that must be assessed case by case [130,131]. Machine-learning (ML) methods are increasingly applied for event reconstruction, particle classification, detector monitoring, and uncertainty quantification. A core methodological requirement is physics-informed validation: ML-assisted results should be benchmarked against controlled simulations and calibration data [132].

The experimental approaches reviewed in this section provide complementary and mutually constraining probes of nuclear symmetries and symmetry breaking. Heavy-ion collisions and charge-exchange reactions constrain the density dependence and spin–isospin response; beta decay and γ spectroscopy elucidate isospin structure, collectivity, and shell evolution; precision masses and parity-violating electron scattering provide comparatively model-robust references for binding-energy trends and neutron-density systematics.

4. Symmetry Energy and Nuclear Astrophysics

The nuclear symmetry energy provides a practical bridge between finite nuclei and bulk neutron-rich matter [22,24,27]. In the standard parabolic expansion of the energy per particle in homogeneous matter [24,27,134],

$$e(n,\delta) = e(n,0) + S(n)\,\delta^2 + \mathcal{O}(\delta^4), \tag{3}$$

the isospin asymmetry is $\delta = (n_n - n_p)/n$ with $n = n_n + n_p$. Here $S(n)$ is the (quadratic) symmetry energy in the parabolic approximation and quantifies the leading isovector contribution, i.e., the energy cost of neutron–proton imbalance at density n [20,21,27]. We recall the standard definitions of J, L, n_s and K_{sym} in Equation (1). While the quadratic term typically dominates around saturation density, higher-order terms can become relevant in very neutron-rich matter at higher densities. Their impact should be propagated as a systematic uncertainty when extrapolating to neutron-star conditions [135,136]. A broad range of analyses suggest a symmetry-energy value at saturation of J in the low-30 MeV range and a slope parameter L of order a few $\times$10 MeV. However, the inferred intervals remain method dependent, reflecting differences in the adopted framework (EDF,

© 2025 by the author(s). Distributed under a Creative Commons CC BY license.

Preprints.org (www.preprints.org) | NOT PEER-REVIEWED | Posted: 19 January 2026 doi:10.20944/preprints202601.1421.v1

chiral EFT, transport-based inference, or astrophysical Bayesian analyses), dataset selection, and prior assumptions [22,24,134]. In the following, we will highlight how constraints on J and L arise from finite nuclei, heavy-ion collisions, and multimessenger observations, and how they propagate to neutron-star radii, tidal deformabilities, and crust properties.

Figure 1 summarizes the inference chain linking symmetry concepts in the isovector sector to laboratory observables, nuclear-matter quantities, and neutron-star properties. The middle step relies on model calibration and statistical inference, so correlations must be interpreted together with theoretical and experimental uncertainties. We denote the neutron-skin thickness by Δr_{np}, the electric dipole polarizability by α_D, and the parity-violating electron scattering asymmetry by $A_{\rm PV}$. For neutron-star observables, $R_{1.4}$ and $\Lambda_{1.4}$ denote the radius and tidal deformability of a 1.4 $M_\odot$ star, respectively.

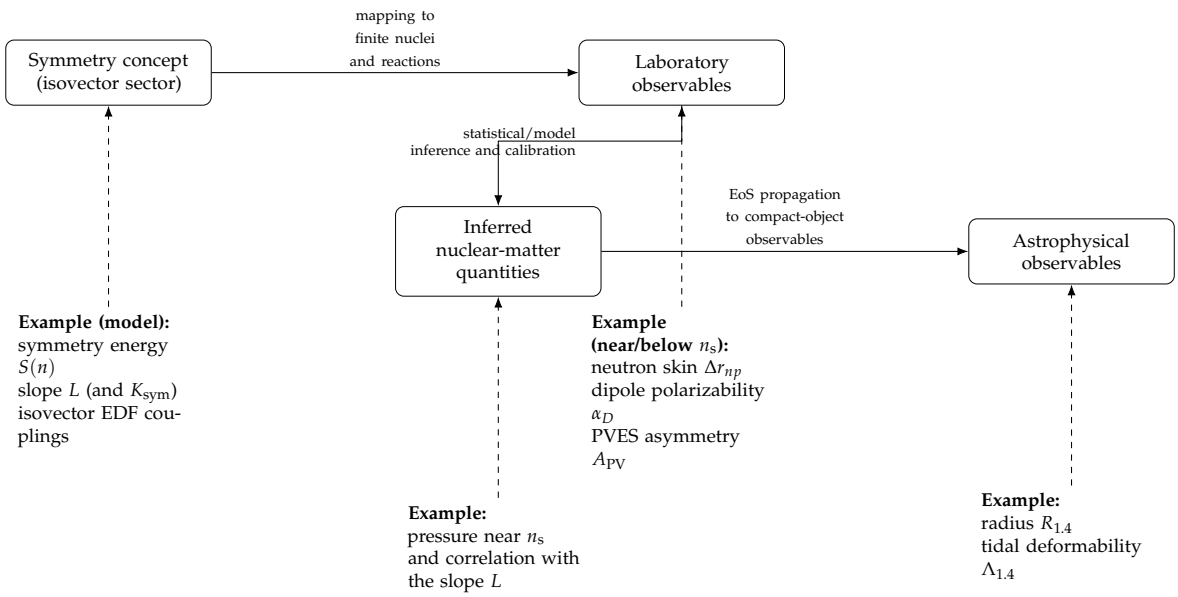

Figure 1. Schematic inference chain linking laboratory observables to neutron-star radii and tidal deformabilities through the isovector sector of the nuclear EoS (illustrated for the symmetry-energy slope L).

4.1. Symmetry Energy at and Below Saturation Density

Hadronic probes, dipole polarizability, isovector giant resonances, and PVES constrain neutron densities and the isovector response, with differing levels of strong-interaction model dependence [22,24,58]. Neutron-skin thicknesses, defined as the difference between neutron and proton rms radii (e.g. in ^{208}Pb and ^{48}Ca), correlate with the pressure of neutron-rich matter near and below saturation density and, within many model families, with the slope parameter L: larger L typically implies thicker skins [22,24,137,138]. The strength and linearity of this correlation are functional- and prior-dependent; thus, quantitative constraints on L should be reported together with the assumed model class and calibration strategy [22]. Isobaric analogue states (IAS) provide a clearer understanding of symmetry coefficients across nuclei when analyzed under charge invariance, and they can be combined consistently with mass information [133]. The systematic studies of the electric dipole polarizability across isotopic chains, combined with EDF and *ab initio* calculations, support well-characterized correlations between α_D, neutron skins, and the density dependence of the symmetry energy [22,62–64]. Low-lying dipole strength (often discussed in terms of pygmy dipole excitations) can add sensitivity to sub-saturation behavior, although its interpretation is more model dependent and should be treated accordingly [22,60,61,64].

4.2. Heavy-Ion Collisions and Symmetry Energy at Finite Temperature

Heavy-ion collisions constrain the isovector sector of the EoS at finite temperature over a broad density range, but only through transport-model interpretations and their associated

© 2025 by the author(s). Distributed under a Creative Commons CC BY license.

Preprints.org (www.preprints.org) | NOT PEER-REVIEWED | Posted: 19 January 2026 doi:10.20944/preprints202601.1421.v1

systematics [81,82,139]. At near-Fermi energies, isospin diffusion in semi-peripheral collisions reflects neutron–proton transport across the low-density neck region. Within transport descriptions, the degree of isospin equilibration is sensitive to the density dependence of the symmetry energy around and below saturation. For many commonly used parameterizations (at fixed J), larger L implies a smaller $S(n)$ at sub-saturation density and can therefore suppress diffusion, with a quantitative mapping that is framework dependent [24,83,86]. Complementary information is provided by isoscaling analyses of fragment yields, which constrain an effective symmetry free-energy coefficient and its temperature dependence; however, the mapping to the underlying symmetry energy depends on assumptions about clustering, secondary decay, and the statistical ensemble [81,82,141]. The synergy between heavy-ion collisions and nuclear structure observables is crucial: structure data constrain the symmetry energy around n_s, while collisions extend sensitivity to finite temperature and, potentially, to supra-saturation densities. The astrophysical relevance is primarily twofold: collisions probe neutron-rich matter away from β equilibrium and at finite T, and they can access densities that overlap with the regime controlling neutron-star radii and tidal deformabilities. Because collisions probe hot, transient matter out of β equilibrium, any astrophysical extrapolation must explicitly account for thermodynamic differences and the framework dependence of the transport-to-EoS mapping [24,139].

4.3. Symmetry Energy, Neutron Stars, and Dense Matter

Neutron stars provide natural laboratories for testing the EoS at densities up to several times saturation, and hence for constraining the symmetry energy within nucleonic and other neutron-rich matter descriptions [25–29,31]. To first approximation, a neutron star consists of a neutron-rich crust and a cold, charge-neutral core in β equilibrium [26,27]. In nucleonic descriptions, the isovector sector of the EoS, including the symmetry energy, plays an important role. At higher densities, where additional degrees of freedom may appear, the mapping to a single "symmetry energy" becomes increasingly composition dependent and should be stated together with the assumed composition. The mass–radius relation is highly sensitive to the EoS. For a given EoS, the Tolman–Oppenheimer–Volkoff equations yield a family of mass–radius curves. The pressure of β-equilibrated matter at around and moderately above saturation influences the radii of typical neutron stars, while the high-density behavior of the EoS largely determines the maximum supported mass [25,27,29]. Observations of neutron stars with masses close to two solar masses therefore set a robust lower bound on the overall stiffness of the EoS at high density [142,143], although this constraint does not by itself isolate the symmetry-energy contribution. At sub-saturation and near-saturation densities, the symmetry energy and its slope govern the pressure of neutron-rich matter and affect the location of the crust–core transition, crust thickness, and the properties of nuclear "pasta" phases. These features can influence crustal oscillations, glitch phenomenology, and cooling behavior, in combination with pairing and neutrino-emission microphysics [26,27]. The dimensionless tidal deformability measured in gravitational-wave events such as GW170817 is sensitive to stellar compactness and thus to the EoS [28,29]. Analyses of GW170817 have yielded bounds on the tidal deformability of a 1.4 $M_\odot$ neutron star [144], constraining the EoS most robustly at intermediate densities relevant for typical radii; sensitivity to the highest-density regime is more prior and parameterization dependent. While the symmetry energy is only one component of the total pressure, its behavior at around and above saturation remains important for neutron-rich matter, particularly within nucleonic EoS models and when assessing possible composition changes with density. In many recent studies, laboratory constraints on the symmetry energy around saturation density are combined with neutron-star mass–radius and tidal-deformability data in Bayesian frameworks to infer posterior distributions for the EoS (and the implied symmetry energy) over a wide density range [27,29,31,86]. These studies generally suggest a moderately stiffening isovector sector with increasing density within nucleonic models, while significant uncertainties remain at higher densities, where additional degrees of freedom may appear and inference outcomes depend strongly on model choices and priors.

© 2025 by the author(s). Distributed under a Creative Commons CC BY license.

Preprints.org (www.preprints.org) | NOT PEER-REVIEWED | Posted: 19 January 2026 doi:10.20944/preprints202601.1421.v1

4.4. Multimessenger Constraints and Consistency Across Scales

Multimessenger astrophysics enables cross-checks across systems and helps tighten constraints on the symmetry energy and the EoS. Gravitational waves from compact binary mergers constrain tidal deformability and thus the equation of state [28,29,144]. Multimessenger analyses, beginning with GW170817 and complemented by NICER pulse-profile modeling, support neutron-star radii of order ∼11–13 km for typical masses within many inference frameworks [29,30]. Neutrino and electromagnetic signals from supernovae and kilonovae depend on the EoS and the symmetry energy, although current constraints remain scenario dependent [27,31] and are entangled with additional physics (e.g., neutrino transport, opacities, composition, and magnetic fields). A notable feature of recent studies is the increasing overlap between laboratory constraints around n_s and multimessenger inferences at the densities most relevant for typical neutron-star radii within nucleonic EoS assumptions; however, several mappings (notably from neutron skins or tidal deformabilities to L) are correlation driven within a chosen theory class, so credible intervals should be reported together with the adopted model class, calibration dataset, and priors [22,24,25,27–29,31,86]. Constraints from finite nuclei, nuclear reactions, and multimessenger observations support a broadly consistent picture of the symmetry energy from sub-saturation densities up to a few times n_s: laboratory data primarily anchor the behavior around n_s, while neutron-star mass–radius and tidal-deformability measurements restrict viable EoS families at higher densities [22,24,25,27–29,31,86]. Significant uncertainties remain at the highest densities, where additional degrees of freedom may appear, but the set of EoS models compatible with current data has narrowed since GW170817.

5. Precision Symmetry Tests and Frontiers Beyond the Standard Model

So far, we have emphasized how symmetry and symmetry breaking organize nuclear structure and connect finite nuclei to neutron stars. We now move to precision tests at the fundamental level, where extremely small symmetry violations can provide strong sensitivity to physics beyond the Standard Model. The aim is to search for effects that are highly suppressed within the Standard Model such as permanent electric dipole moments (EDMs), neutrinoless double-β decay, and parity-violating observables and to translate null results or discoveries into constraints on effective CP-, T-, and lepton-number-violating interactions [2–4,147–149]. Precision studies in nuclei, atoms, and molecules complement studies using high-energy accelerators. High-energy accelerators access new degrees of freedom directly at high momentum transfer, whereas low-energy systems can be highly sensitive to very weak symmetry-violating effects and can probe extremely high effective scales through interference and coherence. The primary challenge is interpretation. The discovery potential of EDM, parity-violation, and $0\nu\beta\beta$ programs relies not only on experimental systematics (background and stability) but also on quantitatively reliable atomic, molecular and nuclear-structure inputs (many-body correlations, operator renormalization, and uncertainty propagation) [2,3,147,149]. Advances in radioactive ion beam production and high-resolution spectroscopy broaden the range of nuclei and molecules that can be exploited for enhanced sensitivity, while electronics developments provide new tools for precision control and readout.

5.1. Time-Reversal Violation and Electric Dipole Moments

A permanent EDM corresponds to an intrinsic separation of positive and negative charge within a system that persists even in the absence of external fields. For a non-degenerate stationary state, a nonzero EDM violates both parity (P) and time-reversal (T) symmetries; assuming CPT invariance, this implies CP violation. Since Standard-Model EDM expectations are many orders of magnitude below present experimental sensitivities, the observation of a nonzero EDM would provide compelling evidence for CP violation beyond the CKM mechanism, potentially arising from, e.g., supersymmetric phases, extended Higgs sectors, leptoquarks, or left–right symmetric interactions [2–4]. Nuclear, atomic, and molecular systems provide particularly stringent EDM probes because symmetry-violating effects can be strongly enhanced by structure and collectivity. Current neutron EDM measurements constrain

© 2025 by the author(s). Distributed under a Creative Commons CC BY license.

Preprints.org (www.preprints.org) | NOT PEER-REVIEWED | Posted: 19 January 2026 doi:10.20944/preprints202601.1421.v1

the neutron EDM to the level of $|d_n| < 1.8 \times 10^{-26}\, e\,\mathrm{cm}$ (90% C.L.) [146], whereas Standard-Model contributions are expected to be many orders of magnitude smaller. Future efforts aim for one–to–two orders of magnitude improvement through increased ultracold-neutron statistics, improved magnetic-field control, and reduced systematic effects [2]. A positive signal in any EDM channel would have major implications for particle physics and cosmology, providing a new source of CP violation potentially relevant to the baryon asymmetry of the Universe [44,45]. In nuclei with octupole deformation ("pear-shaped" nuclei), parity-doublet structures and collective motion can amplify P,T-odd interactions, leading to enhanced nuclear Schiff moments and, consequently, increased sensitivity of atomic EDMs to hadronic sources of CP violation [151–153,155]. Isotopes such as ^{225}Ra are therefore prominent candidates for next-generation searches, and the first atomic-EDM measurement in ^{225}Ra has demonstrated the viability of radioactive-atom techniques in this channel [154]. Complementary enhancement mechanisms arise in certain molecules through nuclear P,T-odd moments such as MQMs (magnetic quadrupole moments) [150].

5.2. Neutrinoless Double-Beta Decay and Lepton-Number Violation

Ordinary double-beta decay ($2\nu\beta\beta$) emits two electrons and two antineutrinos. In the neutrinoless mode ($0\nu\beta\beta$), two neutrons transform into two protons and two electrons without neutrino emission. Observation of $0\nu\beta\beta$ would therefore demonstrate lepton-number violation and, in a model-independent sense, imply that neutrinos have a Majorana component (the "black-box" connection between $0\nu\beta\beta$ and Majorana mass) [157]. $0\nu\beta\beta$ tests whether the neutrino is "its own antiparticle" in the low-energy effective theory. As such, it provides a sensitive probe of lepton-number violation, which is a key ingredient in many scenarios for generating the cosmic matter–antimatter asymmetry (e.g. via leptogenesis), even though the mapping from a low-energy signal to the high-scale origin is mechanism dependent [148,156]. Current searches reach the $\gtrsim 10^{26}$ yr scale in leading isotopes, including ^{136}Xe and ^{76}Ge [158,159]. Next-generation programs such as LEGEND-1000 (Large Enriched Germanium Experiment for Neutrinoless $\beta\beta$ Decay) and nEXO (next Enriched Xenon Observatory) target sensitivities approaching or exceeding $\sim 10^{28}$ yr, corresponding (for light-neutrino exchange) to effective Majorana masses in the $\mathcal{O}(10)$ meV range, with the exact mapping set by nuclear matrix elements and axial-coupling assumptions [160,161]. Interpreting any $0\nu\beta\beta$ signal (or null result) requires reliable nuclear matrix elements (NMEs), which remain a principal theoretical uncertainty. State of the art calculations span large-scale shell-model approaches, quasiparticle random-phase approximation, energy-density-functional methods, and emerging *ab initio* calculations with quantified uncertainties, including efforts based on chiral EFT interactions and consistent weak operators [148,149]. Experimental data including charge-exchange measurements of spin–isospin response and transfer reactions that benchmark pairing and occupancies provide important constraints on "ingredients" of nuclear-structure descriptions and are increasingly used to validate and discriminate NME frameworks, though they do not specifically fix the full $0\nu\beta\beta$ NME on their own [149].

Lastly, although the conventional mechanism is light Majorana neutrino exchange, other short-range or exotic mechanisms (such as heavy sterile neutrino exchange, right-handed currents, or operators mediated by leptoquarks and supersymmetry) may also play a role. Regardless of the predominant underlying mechanism, the positive observation would indicate new physics beyond the Standard Model [148,156].

5.3. Parity Violation and Electroweak Symmetry Tests

Parity violation corresponds to interactions that distinguish left from right. Experimentally, it appears as tiny helicity-dependent asymmetries in otherwise ordinary atomic, nuclear, or scattering observables, driven by the chiral structure of the weak interaction. In electron scattering, parity violation arises from interference between electromagnetic and weak neutral-current amplitudes and provides sensitive low-energy tests of electroweak couplings and possible physics beyond the Standard Model [162–164]. In nuclei, additional parity-violating effects can arise from hadronic weak interactions that mix opposite-parity nuclear states, and in atoms from weak-charge–induced mixing that must

© 2025 by the author(s). Distributed under a Creative Commons CC BY license.

Preprints.org (www.preprints.org) | NOT PEER-REVIEWED | Posted: 19 January 2026 doi:10.20944/preprints202601.1421.v1

be interpreted with high-precision atomic theory [4]. PVES in nuclei primarily constrains neutron distributions. Related measurements also test neutral-current structure and the running of the weak mixing angle, complementing high-energy collider searches. The quantitative interpretation requires controlled electroweak radiative corrections and hadronic and atomic-structure inputs [112,164].

5.4. CPT Symmetry and Precision Antimatter Spectroscopy

CPT symmetry states that physics is unchanged under the combined operations of charge conjugation (C), parity (P), and time reversal (T). It is a cornerstone of local, Lorentz-invariant quantum field theory. Qualitatively, CPT implies that matter and antimatter counterparts have exactly identical masses and (appropriately signed) moments. Atomic and nuclear physics contribute to CPT tests through antihydrogen spectroscopy and Penning-trap comparisons of particle and antiparticle properties. Recent milestones include antihydrogen hyperfine spectroscopy and precision transition measurements in antihydrogen, as well as high-precision proton–antiproton charge-to-mass comparisons and parts-per-billion antiproton magnetic-moment determinations [165–168]. The main challenges are experimental: magnetic-field stability and calibration, trap-related line-shape systematics and long-term control of correlated drifts. Any statistically significant deviation from CPT invariance would challenge the standard theoretical framework and would require either Lorentz-violation scenarios or departures from conventional quantum field theory assumptions [167,168].

5.5. Radioactive Molecules as Precision Symmetry Probes

Molecules containing heavy (and in some cases radioactive) nuclei combine enormous internal effective electric fields with rich level structure. These systems amplify symmetry-violating interactions: a very small effect can produce a comparatively large, measurable signal. Heavy polar molecules have enabled leading searches for the electron EDM (e.g., ThO) and complementary measurements with trapped molecular ions (e.g., HfF^+), while radioactive molecules such as RaF are promising for enhanced sensitivity to hadronic CP violation through nuclear Schiff moments [145,169–171].

5.6. Future Directions in Symmetry Tests

In our opinion, future developments in nuclear symmetry tests will be supported more by consistent, technically challenging improvements in experimental sensitivity and theoretical interpretation than by the introduction of new symmetry notions. In the search for time-reversal and CP violation, EDM experiments are expected to remain a central focus. Improvements in source intensity, trapping efficiency, magnetic-field stability, and background rejection will contribute to enhanced sensitivity. The most promising gains are expected in heavy atoms and molecules and in octupole nuclei, where electronic and collective nuclear structure can amplify CP-odd interactions (e.g., via enhanced Schiff moments) [2–4,150]. As half-life sensitivities for neutrinoless double β decay move toward and beyond 10^{28} years, interpretation becomes increasingly limited by nuclear-structure inputs (matrix elements and effective axial coupling), supporting the coordinated programs that combine decay searches with charge-exchange and two-nucleon transfer constraints and with modern many-body calculations, including chiral-EFT-informed approaches [148,149,156]. Advances in atomic and molecular spectroscopy—particularly in heavy systems—will further expand precision access to parity- and CP-violating observables through level shifts and transition amplitudes that can be extremely difficult to reach in nuclear experiments alone [2,4]. As experimental sensitivities advance, the limiting factor in many symmetry tests will not be the ability to measure small effects, but the confidence with which those effects can be traced back to specific underlying interactions [2,3]. Across all of these areas, progress will depend as strongly on theory as on experiment. Improved uncertainty quantification in nuclear many-body calculations, clearer connections between effective-field-theory interactions and measured observables, and consistent treatments of symmetry breaking and restoration are crucial for drawing robust conclusions from increasingly precise data.

The symmetry tests in nuclear, atomic, and molecular systems will remain a precision-driven science. It will require scrutinizing well-understood observables, often at substantial cost in beam time,

© 2025 by the author(s). Distributed under a Creative Commons CC BY license.

Preprints.org (www.preprints.org) | NOT PEER-REVIEWED | Posted: 19 January 2026 doi:10.20944/preprints202601.1421.v1

detector development, and theoretical effort, while reaching into regimes where even minor symmetry violations would have unambiguous implications for fundamental physics.

6. Conclusions

This review has emphasized symmetry as a unifying notion in nuclear physics, offering a common framework for understanding phenomena ranging from searches for physics beyond the Standard Model to the structure of finite nuclei and neutron-star properties. Approximate symmetries in nuclei, including isospin, pseudospin, and collective dynamical symmetries associated with SU(3) and $\mathrm{Sp}(3,\mathbb{R})$, play a central role in shaping spectra, transition patterns, and emergent regularities. Their systematic breaking – through Coulomb effects, shell evolution, continuum coupling, and spin–orbit coupling is more than just a difficulty. It provides detailed and often quantitative information on the effective nuclear interaction and correlated many-body motion. Recent advances in high-resolution γ spectroscopy, charge-exchange reactions, precision mass measurements, and radioactive-ion-beam experiments have improved our ability to isolate and quantify such effects, especially in regions far from stability where weak binding and strong isospin asymmetry amplify both structure and symmetry breaking. At the macroscopic level, the nuclear symmetry energy provides a direct bridge between finite nuclei and neutron-rich matter in astrophysical environments. Constraints from neutron skins, dipole polarizability, and heavy-ion collisions are increasingly compared with those inferred from neutron-star mass–radius measurements, tidal deformabilities from gravitational waves, and X-ray timing. This emerging convergence has begun to narrow the range of feasible equations of state near saturation density and often favors moderately stiff behavior within nucleonic EoS families. However, mapping from observables to EoS parameters remains correlation- and model-class dependent; credible intervals must therefore be quoted together with the assumed parameterization, composition, and prior choices. Important uncertainties persist at supra-saturation densities, where additional degrees of freedom and phase transitions may become relevant. Nuclear, atomic, and molecular systems can amplify extremely small symmetry-violating effects and thereby provide sensitive probes of CP violation and physics beyond the Standard Model. Searches for electric dipole moments, neutrinoless double-β decay, and parity-violating observables continue to push experimental sensitivity into regimes that are complementary to high-energy collider probes. The limiting factor is not the measurement itself but the confidence with which a null result or discovery can be traced back to specific underlying operators. This emphasizes the need for nuclear many-body theory with controlled theoretical errors and transparent uncertainty quantification. Next-generation rare isotope facilities will extend reach toward the most neutron-rich and proton-rich systems, while continued improvements in detector technology, beam delivery, and data-analysis methods will reduce systematic uncertainties that currently limit symmetry-based constraints. On the theory side, sustained integration of *ab initio* approaches, EDF methods, and astrophysical modeling with consistent treatments of symmetry breaking and restoration will be needed to maintain coherence between laboratory observables and dense-matter phenomenology. Symmetry transcends mere classification; it helps relate different measurements, identifies robust correlations, and reveals the limitations of current models. Nuclear physics provides insight into the structure of matter and the governing interactions across scales, from nuclei to neutron stars, by investigating the conditions under which symmetries hold and fail.

Author Contributions: Conceptualization, J.V.; writing/original draft preparation, J.V.; writing/review and editing, J.V.

Funding: This research was funded by Slovenian Research and Innovation Agency, grant numbers: P1-0102, I0-E005.

Data Availability Statement: Not applicable.

Conflicts of Interest: The author declares no conflict of interest.

© 2025 by the author(s). Distributed under a Creative Commons CC BY license.

Preprints.org (www.preprints.org) | NOT PEER-REVIEWED | Posted: 19 January 2026 doi:10.20944/preprints202601.1421.v1

References

1. Noether, E. Invariante Variationsprobleme. *Nachr. Ges. Wiss. Göttingen, Math.-Phys. Kl.* **1918**, 235–257. (English translation: Tavel, M.A. *Transp. Theory Stat. Phys.* **1971**, *1*, 183–207.)
2. Chupp, T.E.; Fierlinger, P.; Ramsey-Musolf, M.J.; Singh, J.T. Electric dipole moments of atoms, molecules, nuclei, and particles. *Rev. Mod. Phys.* **2019**, *91*, 015001. doi:10.1103/RevModPhys.91.015001.
3. Engel, J.; Ramsey-Musolf, M.J.; van Kolck, U. Electric Dipole Moments of Nucleons, Nuclei, and Atoms: The Standard Model and Beyond. *Prog. Part. Nucl. Phys.* **2013**, *71*, 21–74. doi:10.1016/j.ppnp.2013.03.003.
4. Safronova, M.S.; Budker, D.; DeMille, D.; Kimball, D.F.J.; Derevianko, A.; Clark, C.W. Search for New Physics with Atoms and Molecules. *Rev. Mod. Phys.* **2018**, *90*, 025008. doi:10.1103/RevModPhys.90.025008.
5. Heisenberg, W. Über den Bau der Atomkerne. I. *Z. Phys.* **1932**, *77*, 1–11. doi:10.1007/BF01342433.
6. Wigner, E.P. On the Consequences of the Symmetry of the Nuclear Hamiltonian on the Spectroscopy of Nuclei. *Phys. Rev.* **1937**, *51*, 106–119. doi:10.1103/PhysRev.51.106.
7. Miller, G.A.; Opper, A.K.; Stephenson, E.J. Charge Symmetry Breaking and QCD. *Annu. Rev. Nucl. Part. Sci.* **2006**, *56*, 253–292. doi:10.1146/annurev.nucl.56.080805.140446.
8. Bentley, M.A.; Lenzi, S.M. Coulomb energy differences between high-spin states in isobaric multiplets. *Prog. Part. Nucl. Phys.* **2007**, *59*, 497–561. doi:10.1016/j.ppnp.2006.10.001.
9. Taddeucci, T.N.; Goulding, C.A.; Carey, T.A.; et al. The (p,n) reaction as a probe of beta decay strength. *Nucl. Phys. A* **1987**, *469*, 125–172. doi:10.1016/0375-9474(87)90089-3.
10. Osterfeld, F. *Nuclear spin and isospin excitations.* *Rev. Mod. Phys.* **1992**, *64*, 491–557. doi:10.1103/RevModPhys.64.491.
11. Ichimura, M.; Sakai, H.; Wakasa, T. Spin–isospin responses via (p,n) and (n,p) reactions. *Prog. Part. Nucl. Phys.* **2006**, *56*, 446–531. doi:10.1016/j.ppnp.2005.09.001.
12. Elliott, J.P. Collective Motion in the Nuclear Shell Model. I. Classification Schemes for States of Mixed Configurations. *Proc. R. Soc. Lond. A* **1958**, *245*, 128–145. doi:10.1098/rspa.1958.0072.
13. Elliott, J.P. Collective Motion in the Nuclear Shell Model. II. The Introduction of Intrinsic Wave-Functions. *Proc. R. Soc. Lond. A* **1958**, *245*, 562–581. doi:10.1098/rspa.1958.0101.
14. Rowe, D.J.; Wood, J.L. *Fundamentals of Nuclear Models: Foundational Models*; World Scientific: Singapore, 2010. doi:10.1142/6209.
15. Launey, K.D.; Dytrych, T.; Draayer, J.P. Symmetry-Guided Large-Scale Shell-Model Theory. *Prog. Part. Nucl. Phys.* **2016**, *89*, 101–136. doi:10.1016/j.ppnp.2016.02.001.
16. Pietralla, N.; von Brentano, P.; Lisetskiy, A.F. Experiments on multiphonon states with proton–neutron mixed symmetry in vibrational nuclei. *Prog. Part. Nucl. Phys.* **2008**, *60*, 225–282. doi:10.1016/j.ppnp.2007.08.002.
17. Ginocchio, J.N. Pseudospin as a Relativistic Symmetry. *Phys. Rev. Lett.* **1997**, *78*, 436–439. doi:10.1103/PhysRevLett.78.436.
18. Van Isacker, P.; Heyde, K.; Jolie, J.; Sevrin, A. The F-spin symmetric limits of the neutron-proton interacting boson model. *Ann. Phys.* **1986**, *171*, 253–296. doi:10.1016/0003-4916(86)90002-3.
19. Dieperink, A.E.L.; van Isacker, P. The symmetry energy in nuclei and in nuclear matter. *Eur. Phys. J. A* **2007**, *32*, 11–18. doi:10.1140/epja/i2007-10360-3.
20. Hebeler, K.; Holt, J.D.; Menéndez, J.; Schwenk, A. Nuclear Forces and Their Impact on Neutron-Rich Nuclei and Neutron-Rich Matter. *Annu. Rev. Nucl. Part. Sci.* **2015**, *65*, 457–484. doi:10.1146/annurev-nucl-102313-025446.
21. Drischler, C.; Furnstahl, R.J.; Meléndez, J.A.; Phillips, D.R. How Well Do We Know the Neutron-Matter Equation of State at the Densities Inside Neutron Stars? A Bayesian Approach with Correlated Uncertainties. *Phys. Rev. Lett.* **2020**, *125*, 202702. doi:10.1103/PhysRevLett.125.202702.
22. Roca-Maza, X.; Paar, N. Nuclear Equation of State from Ground and Collective Excited State Properties of Nuclei. *Prog. Part. Nucl. Phys.* **2018**, *101*, 96–176. doi:10.1016/j.ppnp.2018.04.001.
23. Horowitz, C.J.; Ahmed, Z.; Jen, C.-M.; et al. Weak Charge Form Factor and Radius of ^{208}Pb through Parity Violation in Electron Scattering. *Phys. Rev. C* **2012**, *85*, 032501. doi:10.1103/PhysRevC.85.032501.
24. Tsang, M.B.; Stone, J.R.; Camera, F.; Danielewicz, P.; Gandolfi, S.; Hebeler, K.; Horowitz, C.J.; Lee, J.; Lynch, W.G.; et al. Constraints on the symmetry energy and neutron skins from experiments and theory. *Phys. Rev. C* **2012**, *86*, 015803. doi:10.1103/PhysRevC.86.015803.
25. Lattimer, J.M.; Steiner, A.W. Constraints on the Symmetry Energy Using the Mass-Radius Relation of Neutron Stars. *Eur. Phys. J. A* **2014**, *50*, 40. doi:10.1140/epja/i2014-14040-y.
26. Lattimer, J.M.; Prakash, M. The Physics of Neutron Stars. *Science* **2004**, *304*, 536–542. doi:10.1126/science.1090720.

© 2025 by the author(s). Distributed under a Creative Commons CC BY license.

Preprints.org (www.preprints.org) | NOT PEER-REVIEWED | Posted: 19 January 2026 doi:10.20944/preprints202601.1421.v1

27. Oertel, M.; Hempel, M.; Klähn, T.; Typel, S. Equations of State for Supernovae and Compact Stars. *Rev. Mod. Phys.* **2017**, *89*, 015007. doi:10.1103/RevModPhys.89.015007.
28. Abbott, B.P.; et al. (LIGO Scientific Collaboration and Virgo Collaboration). GW170817: Observation of Gravitational Waves from a Binary Neutron Star Inspiral. *Phys. Rev. Lett.* **2017**, *119*, 161101. doi:10.1103/PhysRevLett.119.161101.
29. Annala, E.; Gorda, T.; Kurkela, A.; Vuorinen, A. Gravitational-Wave Constraints on the Neutron-Star Matter Equation of State. *Phys. Rev. Lett.* **2018**, *120*, 172703. doi:10.1103/PhysRevLett.120.172703.
30. Riley, T.E.; Watts, A.L.; Bogdanov, S.; Ray, P.S.; Guillot, S.; Arzoumanian, Z.; Ballantyne, D.R.; Belloni, T.; Bhattacharyya, S.; Bilous, A.V.; et al. A NICER View of PSR J0030+0451: Millisecond Pulsar Parameter Estimation. *Astrophys. J. Lett.* **2019**, *887*, L21. doi:10.3847/2041-8213/ab481c.
31. Li, B.A.; Krastev, P.G.; Wen, D.H.; Zhang, N.B. Towards Understanding the Astrophysical Effects of Nuclear Symmetry Energy. *Eur. Phys. J. A* **2019**, *55*, 117. doi:10.1140/epja/i2019-12780-8.
32. Fattoyev, F.J.; Piekarewicz, J.; Horowitz, C.J. Neutron Skins and Neutron Stars in the Multimessenger Era. *Phys. Rev. Lett.* **2018**, *120*, 172702. doi:10.1103/PhysRevLett.120.172702.
33. Fujita, Y.; Rubio, B.; Gelletly, W. Spin–isospin excitations probed by strong, weak and electromagnetic interactions. *Prog. Part. Nucl. Phys.* **2011**, *66*, 549–606. doi:10.1016/j.ppnp.2011.01.056.
34. Fujita, Y.; Fujita, H.; Rubio, B.; Gelletly, W.; Blank, B. Gamow–Teller Transitions — a Mirror Reflecting Nuclear Structure. *Acta Phys. Pol. B* **2012**, *43*, 153–166. doi:10.5506/APhysPolB.43.153.
35. Fujita, H.; Fujita, Y.; Adachi, T.; et al. Isospin mixing of the isobaric analog state studied in a high-resolution ^{56}Fe(^{3}He,t)^{56}Co reaction. *Phys. Rev. C* **2013**, *88*, 054329. doi:10.1103/PhysRevC.88.054329.
36. Diel, F.; Fujita, Y.; Fujita, H.; Cappuzzello, F.; Ganioğlu, E.; et al. High-resolution study of the Gamow–Teller (GT^{-}) strength in the ^{64}Zn(^{3}He,t)^{64}Ga reaction. *Phys. Rev. C* **2019**, *99*, 054322. doi:10.1103/PhysRevC.99.054322.
37. Blaum, K. High-accuracy mass spectrometry with stored ions. *Phys. Rep.* **2006**, *425*, 1–78. doi:10.1016/j.physrep.2005.10.011.
38. Campbell, P.; Moore, I.D.; Pearson, M.R. Laser spectroscopy for nuclear structure physics. *Prog. Part. Nucl. Phys.* **2016**, *86*, 127–180. doi:10.1016/j.ppnp.2015.09.003.
39. Litvinov, Y.A.; Bosch, F. Beta decay of highly charged ions. *Rep. Prog. Phys.* **2011**, *74*, 016301. doi:10.1088/0034-4885/74/1/016301.
40. Palit, R.; Saha, S.; Sethi, J.; Trivedi, T.; Sharma, S.; Naidu, B.S.; Jadhav, S.; Donthi, R.; Chavan, P.B.; Tan, H.; Hennig, W. A high speed digital data acquisition system for the Indian National Gamma Array at Tata Institute of Fundamental Research. *Nucl. Instrum. Methods Phys. Res. A* **2012**, *680*, 90–96. doi:10.1016/j.nima.2012.03.046.
41. Korten, W.; Atac, A.; Beaumel, D.; Bednarczyk, P.; Bentley, M.A.; Benzoni, G.; Boston, A.; Bracco, A.; Cederkäll, J.; Cederwall, B.; et al. (the AGATA Collaboration) Physics opportunities with the Advanced Gamma Tracking Array: AGATA. *Eur. Phys. J. A* **2020**, *56*, 137. doi:10.1140/epja/s10050-020-00132-w.
42. Hennig, A.; Spieker, M.; Werner, V.; Ahn, T.; Anagnostatou, V.; Cooper, N.; Derya, V.; Elvers, M.; Endres, J.; Goddard, P.; Heinz, A.; Hughes, R.O.; Ilie, G.; Mineva, M.N.; Petkov, P.; Pickstone, S.G.; Pietralla, N.; Radeck, D.; Ross, T.J.; Savran, D.; Zilges, A. *Mixed-Symmetry Octupole and Hexadecapole Excitations in the $N = 52$ Isotones.* *Phys. Rev. C* **2014**, *90*, 051302(R). doi:10.1103/PhysRevC.90.051302.
43. Epelbaum, E.; Hammer, H.-W.; Meißner, U.-G. Modern Theory of Nuclear Forces. *Rev. Mod. Phys.* **2009**, *81*, 1773–1825. doi:10.1103/RevModPhys.81.1773.
44. Dine, M.; Kusenko, A. The Origin of the Matter–Antimatter Asymmetry. *Rev. Mod. Phys.* **2003**, *76*, 1–30. doi:10.1103/RevModPhys.76.1.
45. Riotto, A.; Trodden, M. Recent Progress in Baryogenesis. *Annu. Rev. Nucl. Part. Sci.* **1999**, *49*, 35–75. doi:10.1146/annurev.nucl.49.1.35.
46. Lee, T.D.; Yang, C.N. Question of Parity Conservation in Weak Interactions. *Phys. Rev.* **1956**, *104*, 254–258. doi:10.1103/PhysRev.104.254.
47. Wu, C.S.; Ambler, E.; Hayward, R.W.; Hoppes, D.D.; Hudson, R.P. Experimental Test of Parity Conservation in Beta Decay. *Phys. Rev.* **1957**, *105*, 1413–1415. doi:10.1103/PhysRev.105.1413.
48. Lüders, G. On the Equivalence of Invariance under Time Reversal and under Particle–Antiparticle Conjugation for Relativistic Field Theories. *Dan. Mat. Fys. Medd.* **1954**, *28*, No. 5.
49. Pauli, W. Exclusion Principle, Lorentz Group and Reflection of Space-Time and Charge. In *Niels Bohr and the Development of Physics*; Pauli, W., Ed.; Pergamon Press: London, UK, 1955; pp. 30–51.

© 2025 by the author(s). Distributed under a Creative Commons CC BY license.

Preprints.org (www.preprints.org) | NOT PEER-REVIEWED | Posted: 19 January 2026 doi:10.20944/preprints202601.1421.v1

50. Navas, S.; et al. (Particle Data Group). *Review of Particle Physics. Phys. Rev. D* **2024**, *110*, 030001. doi:10.1103/PhysRevD.110.030001.
51. Sun, L.J.; Xu, X.X.; Lin, C.J.; Lee, J.; Hou, S.Q.; Yuan, C.X.; Li, Z.H.; José, J.; He, J.J.; et al. (RIBLL Collaboration). *β-Decay Spectroscopy of* ^{27}*S. Phys. Rev. C* **2019**, *99*, 064312. doi:10.1103/PhysRevC.99.064312.
52. Bentley, M.A.; Lenzi, S.M.; Simpson, S.A.; Diget, C.Aa. *Isospin-Breaking Interactions Studied through Mirror Energy Differences. Phys. Rev. C* **2015**, *92*, 024310. doi:10.1103/PhysRevC.92.024310.
53. Auerbach, N. *Coulomb Effects in Nuclear Structure. Phys. Rep.* **1983**, *98*, 273–341. doi:10.1016/0370-1573(83)90008-X.
54. Ehrman, J.B. *On the Displacement of Corresponding Energy Levels of* ^{13}*C and* ^{13}*N. Phys. Rev.* **1951**, *81*, 412–416. doi:10.1103/PhysRev.81.412.
55. Thomas, R.G. *An Analysis of the Energy Levels of the Mirror Nuclei,* ^{13}*C and* ^{13}*N. Phys. Rev.* **1952**, *88*, 1109–1125. doi:10.1103/PhysRev.88.1109.
56. MacCormick, M.; Audi, G. *Evaluated Experimental Isobaric Analogue States from* $T = 1/2$ *to* $T = 3$ *and Associated IMME Coefficients. Nucl. Phys. A* **2014**, *925*, 61–95. doi:10.1016/j.nuclphysa.2014.01.007.
57. Bender, M.; Heenen, P.-H.; Reinhard, P.-G. Self-consistent mean-field models for nuclear structure. *Rev. Mod. Phys.* **2003**, *75*, 121–180. doi:10.1103/RevModPhys.75.121.
58. Harakeh, M.N.; van der Woude, A. *Giant Resonances: Fundamental High-Frequency Modes of Nuclear Excitation*; Oxford University Press: Oxford, UK, 2001; ISBN 978-0-19-851733-7.
59. Garg, U.; Colò, G. *The Compression-Mode Giant Resonances and Nuclear Incompressibility. Prog. Part. Nucl. Phys.* **2018**, *101*, 55–95. doi:10.1016/j.ppnp.2018.03.001.
60. Piekarewicz, J. *Pygmy Dipole Resonance as a Constraint on the Neutron Skin of Heavy Nuclei. Phys. Rev. C* **2006**, *73*, 044325. doi:10.1103/PhysRevC.73.044325.
61. Savran, D.; Aumann, T.; Zilges, A. *Experimental Studies of the Pygmy Dipole Resonance. Prog. Part. Nucl. Phys.* **2013**, *70*, 210–245. doi:10.1016/j.ppnp.2013.02.003.
62. Reinhard, P.-G.; Nazarewicz, W. *Information Content of a New Observable: The Case of the Nuclear Neutron Skin. Phys. Rev. C* **2010**, *81*, 051303(R). doi:10.1103/PhysRevC.81.051303.
63. Tamii, A.; Poltoratska, I.; von Neumann-Cosel, P.; Fujita, Y.; Adachi, T.; Bertulani, C.A.; et al. *Complete Electric Dipole Response and the Neutron Skin in* ^{208}*Pb. Phys. Rev. Lett.* **2011**, *107*, 062502. doi:10.1103/PhysRevLett.107.062502.
64. Piekarewicz, J.; Agrawal, B.K.; Colò, G.; Nazarewicz, W.; Paar, N.; Reinhard, P.-G.; Roca-Maza, X.; Vretenar, D. *Electric Dipole Polarizability and the Neutron Skin. Phys. Rev. C* **2012**, *85*, 041302(R). doi:10.1103/PhysRevC.85.041302.
65. Ginocchio, J.N. Relativistic symmetries in nuclei and hadrons. *Phys. Rep.* **2005**, *414*, 165–261. doi:10.1016/j.physrep.2005.04.003.
66. Liang, H.; Meng, J.; Zhou, S.-G. *Hidden Pseudospin and Spin Symmetries and Their Origins in Atomic Nuclei. Phys. Rep.* **2015**, *570*, 1–84. doi:10.1016/j.physrep.2014.12.005.
67. Iachello, F.; Arima, A. *The Interacting Boson Model*; Cambridge University Press: Cambridge, UK, 1987.
68. Coquard, L.; Pietralla, N.; Rainovski, G.; Ahn, T.; Bettermann, L.; Carpenter, M.P.; Janssens, R.V.F.; Leske, J.; Lister, C.J.; et al. *Evolution of the Mixed-Symmetry* $2^+_{1,\mathrm{ms}}$ *Quadrupole-Phonon Excitation from Spherical to* γ*-Soft Xe Nuclei. Phys. Rev. C* **2010**, *82*, 024317. doi:10.1103/PhysRevC.82.024317.
69. Freer, M.; Horiuchi, H.; Kanada-En'yo, Y.; Lee, D.; Meißner, U.-G. *Microscopic Clustering in Light Nuclei. Rev. Mod. Phys.* **2018**, *90*, 035004. doi:10.1103/RevModPhys.90.035004.
70. Frederico, T.; Delfino, A.; Tomio, L.; Yamashita, M.T. *Universal Aspects of Light Halo Nuclei. Prog. Part. Nucl. Phys.* **2012**, *67*, 939–994. doi:10.1016/j.ppnp.2012.06.001.
71. Heyde, K.; Wood, J.L. *Shape Coexistence in Atomic Nuclei. Rev. Mod. Phys.* **2011**, *83*, 1467–1521. doi:10.1103/RevModPhys.83.1467.
72. Frauendorf, S.; Macchiavelli, A.O. Overview of neutron–proton pairing. *Prog. Part. Nucl. Phys.* **2014**, *78*, 24–90. doi:10.1016/j.ppnp.2014.07.001.
73. Cederwall, B.; Ghazi Moradi, F.; Bäck, T.; Johnson, A.; Blomqvist, J.; Clément, E.; et al. *Evidence for a Spin-Aligned Neutron–Proton Paired Phase from the Level Structure of* ^{92}*Pd. Nature* **2011**, *469*, 68–71. doi:10.1038/nature09644.
74. Talmi, I. *Simple Models of Complex Nuclei: The Shell Model and Interacting Boson Model*; Harwood Academic Publishers: Chur, Switzerland, 1993.
75. Weinberg, S. *Nuclear Forces from Chiral Lagrangians. Phys. Lett. B* **1990**, *251*, 288–292. doi:10.1016/0370-2693(90)90938-3.

© 2025 by the author(s). Distributed under a Creative Commons CC BY license.

Preprints.org (www.preprints.org) | NOT PEER-REVIEWED | Posted: 19 January 2026 doi:10.20944/preprints202601.1421.v1

76. Weinberg, S. *Effective Chiral Lagrangians for Nucleon–Pion Interactions and Nuclear Forces. Nucl. Phys. B* **1991**, *363*, 3–18. doi:10.1016/0550-3213(91)90231-L.
77. Machleidt, R.; Entem, D.R. *Chiral Effective Field Theory and Nuclear Forces. Phys. Rep.* **2011**, *503*, 1–75. doi:10.1016/j.physrep.2011.02.001.
78. Krebs, H. Nuclear currents in chiral effective field theory. *Eur. Phys. J. A* **2020**, *56*, 234. doi:10.1140/epja/s10050-020-00230-9.
79. Hammer, H.-W.; König, S.; van Kolck, U. *Nuclear Effective Field Theory: Status and Perspectives. Rev. Mod. Phys.* **2020**, *92*, 025004. doi:10.1103/RevModPhys.92.025004.
80. Ring, P.; Schuck, P. *The Nuclear Many-Body Problem*; Theoretical and Mathematical Physics; Springer-Verlag: Berlin, Heidelberg, Germany, 1980; ISBN 3-540-09820-8.
81. Li, B.A.; Chen, L.W.; Ko, C.M. Recent Progress and New Challenges in Isospin Physics with Heavy-Ion Reactions. *Phys. Rep.* **2008**, *464*, 113–281. doi:10.1016/j.physrep.2008.04.005.
82. Baran, V.; Colonna, M.; Greco, V.; Di Toro, M. Reaction Dynamics with Exotic Beams. *Phys. Rep.* **2005**, *410*, 335–466. doi:10.1016/j.physrep.2004.12.004.
83. Tsang, M.B.; Liu, T.X.; Shi, L.; et al. Isospin Diffusion and the Nuclear Symmetry Energy in Heavy-Ion Reactions. *Phys. Rev. Lett.* **2004**, *92*, 062701. doi:10.1103/PhysRevLett.92.062701.
84. Aumann, T.; Bertulani, C.A.; Schindler, F.; Typel, S. Peeling Off Neutron Skins from Neutron-Rich Nuclei: Constraints on the Symmetry Energy from Neutron-Removal Cross Sections. *Phys. Rev. Lett.* **2017**, *119*, 262501. doi:10.1103/PhysRevLett.119.262501.
85. Danielewicz, P.; Lacey, R.; Lynch, W.G. Determination of the Equation of State of Dense Matter. *Science* **2002**, *298*, 1592–1596. doi:10.1126/science.1078070.
86. Li, B.-A.; Ramos, À.; Verde, G.; Vidaña, I. Topical Issue on Nuclear Symmetry Energy. *Eur. Phys. J. A* **2014**, *50*, 9. doi:10.1140/epja/i2014-14009-x.
87. Xiao, Z.; Li, B.-A.; Chen, L.-W.; Yong, G.-C.; Zhang, M. Circumstantial Evidence for a Soft Nuclear Symmetry Energy at Suprasaturation Densities. *Phys. Rev. Lett.* **2009**, *102*, 062502. doi:10.1103/PhysRevLett.102.062502.
88. Xiao, Z.-G.; Yong, G.-C.; Chen, L.-W.; Li, B.-A.; Zhang, M.; Xiao, G.-Q.; Xu, N. Probing Nuclear Symmetry Energy at High Densities Using Pion, Kaon, Eta and Photon Productions in Heavy-Ion Collisions. *Eur. Phys. J. A* **2014**, *50*, 37. doi:10.1140/epja/i2014-14037-6.
89. Ferini, G.; Gaitanos, T.; Colonna, M.; Di Toro, M.; Wolter, H.H. Isospin Effects on Subthreshold Kaon Production at Intermediate Energies. *Phys. Rev. Lett.* **2006**, *97*, 202301. doi:10.1103/PhysRevLett.97.202301.
90. Yong, G.-C.; Li, B.-A.; Chen, L.-W. Neutron–Proton Bremsstrahlung from Intermediate-Energy Heavy-Ion Reactions as a Probe of the Nuclear Symmetry Energy? *Phys. Lett. B* **2008**, *661*, 82–87. doi:10.1016/j.physletb.2008.02.013.
91. Russotto, P.; Gannon, S.; Kupny, S.; Lasko, P.; Acosta, L.; Adamczyk, M.; Al-Ajlan, A.; Al-Garawi, M.; Al-Homaidhi, S.; et al. Results of the ASY-EoS Experiment at GSI: The Symmetry Energy at Suprasaturation Density. *Phys. Rev. C* **2016**, *94*, 034608. doi:10.1103/PhysRevC.94.034608.
92. Kobayashi, T.; Chiga, N.; Isobe, T.; Kondo, Y.; Kubo, T.; Kusaka, K.; Motobayashi, T.; Nakamura, T.; Ohnishi, J.; Okuno, H.; Otsu, H.; Sako, T.; Sato, H.; Shimizu, Y.; Sekiguchi, K.; Takahashi, K.; Tanaka, R.; Yoneda, K. SAMURAI Spectrometer for RI Beam Experiments. *Nucl. Instrum. Methods Phys. Res. B* **2013**, *317*, 294–304. doi:10.1016/j.nimb.2013.05.089.
93. Hong, B.; Ahn, D.S.; Ahn, J.K.; Bae, J.; Bae, Y.; Bok, J.S.; Choi, S.W.; Do, S.; Heo, C.; Huh, J.; Hwang, J.; Jang, Y.; Kang, B.; Kim, A.; Kim, B.K.; Kim, C.; Kim, E.-J.; Kim, G.W.; Kim, G.Y.; Kim, H.C.; Kim, H.M.; Yang, H.M.; et al. Status of LAMPS at RAON. *Nucl. Instrum. Methods Phys. Res. B* **2023**, *541*, 260–263. doi:10.1016/j.nimb.2023.05.030.
94. Fujiwara, M.; Akimune, H.; Daito, I.; Fujimura, H.; Fujita, Y.; Hatanaka, K.; Ikegami, H.; Katayama, I.; Nagayama, K.; Matsuoka, N.; Morinobu, S.; Noro, T.; Yoshimura, M.; Sakaguchi, H.; Sakemi, Y.; Tamii, A.; Yosoi, M. Magnetic Spectrometer Grand Raiden. *Nucl. Instrum. Methods Phys. Res. A* **1999**, *422*, 484–488. doi:10.1016/S0168-9002(98)01009-2.
95. Neveling, R. Opportunities with the K600 Magnetic Spectrometer During Phase 1 of the iThemba LABS RIB Project. In *Exotic Nuclei IASEN-2013: Proceedings of the First International African Symposium on Exotic Nuclei*; Cherepanov, E.; Penionzhkevich, Y.; Kamanin, D.; Bark, R.; Cornell, J., Eds.; World Scientific: Singapore, 2015; pp. 181–189. doi:10.1142/9789814632041_0018.
96. Xu, J.; Chen, L.-W.; Tsang, M.B.; Wolter, H.; Zhang, Y.-X.; Aichelin, J.; et al. Understanding Transport Simulations of Heavy-Ion Collisions at 100A and 400A MeV: Comparison of Heavy-Ion Transport Codes under Controlled Conditions. *Phys. Rev. C* **2016**, *93*, 044609. doi:10.1103/PhysRevC.93.044609.

© 2025 by the author(s). Distributed under a Creative Commons CC BY license.

Preprints.org (www.preprints.org) | NOT PEER-REVIEWED | Posted: 19 January 2026 doi:10.20944/preprints202601.1421.v1

97. Cortesi, M.; Pereira, J.; Bazin, D.; Ayyad, Y.; Cerizza, G.; Fox, R.; Zegers, R.G.T. Development of a novel MPGD-based drift chamber for the NSCL/FRIB S800 spectrometer. *JINST* **2020**, *15*, P03025. doi:10.1088/1748-0221/15/03/P03025.
98. Shimbara, Y.; Fujita, Y.; Yoshida, K.; et al. High-Resolution Study of Gamow–Teller Transitions with the ^{37}Cl(^{3}He,t)^{37}Ar Reaction. *Phys. Rev. C* **2012**, *86*, 024312. doi:10.1103/PhysRevC.86.024312.
99. Langanke, K.; Martínez-Pinedo, G. Nuclear Weak-Interaction Processes in Stars. *Rev. Mod. Phys.* **2003**, *75*, 819–862. doi:10.1103/RevModPhys.75.819.
100. Hardy, J.C.; Towner, I.S. *Superallowed* $0^+ \to 0^+$ *nuclear beta decays: 2020 critical survey, with implications for* V_{ud} *and CKM unitarity. Phys. Rev. C* **2020**, *102*, 045501. doi:10.1103/PhysRevC.102.045501.
101. Büscher, J.; Ponsaers, J.; Raabe, R.; Huyse, M.; Van Duppen, P.; et al. β-Decay Studies with an Implantation Technique. *Nucl. Instrum. Methods Phys. Res. B* **2008**, *266*, 4652–4656. doi:10.1016/j.nimb.2008.05.084.
102. Blank, B.; Borge, M.J.G. Nuclear Structure at the Proton Drip Line: Advances with Nuclear Decay Studies. *Prog. Part. Nucl. Phys.* **2008**, *60*, 403–483. doi:10.1016/j.ppnp.2007.12.001.
103. Pfützner, M.; Karny, M.; Grigorenko, L.V.; Riisager, K. Radioactive Decays at Limits of Nuclear Stability. *Rev. Mod. Phys.* **2012**, *84*, 567–619. doi:10.1103/RevModPhys.84.567.
104. Hall, O.; Davinson, T.; Griffin, C.J.; Woods, P.J.; et al. The Advanced Implantation Detector Array (AIDA). *Nucl. Instrum. Methods Phys. Res. A* **2023**, *1050*, 168166. doi:10.1016/j.nima.2023.168166.
105. Lee, I.Y. *The GAMMASPHERE. Nucl. Phys. A* **1990**, *520*, 641c–655c. doi:10.1016/0375-9474(90)91181-P.
106. Muralithar, S.; Rani, K.; Kumar, R.; Singh, R.P.; et al. *Indian National Gamma Array at Inter University Accelerator Centre, New Delhi. Nucl. Instrum. Methods Phys. Res. A* **2010**, *622*, 281–287. doi:10.1016/j.nima.2010.06.200.
107. Lee, I.Y.; Clark, R.M.; et al. *GRETINA: A gamma ray energy tracking array. Nucl. Phys. A* **2004**, *746*, 255–259. doi:10.1016/j.nuclphysa.2004.09.038.
108. Paschalis, S.; et al. *The performance of the Gamma-Ray Energy Tracking In-beam Nuclear Array GRETINA. Nucl. Instrum. Methods Phys. Res. A* **2013**, *709*, 44–55. doi:10.1016/j.nima.2013.01.009.
109. Dewald, A.; Möller, O.; Petkov, P. *Developing the Recoil Distance Doppler-Shift technique towards a versatile tool for lifetime measurements of excited nuclear states. Prog. Part. Nucl. Phys.* **2012**, *67*, 786–839. doi:10.1016/j.ppnp.2012.03.003.
110. Régis, J.-M.; Fraile, L.M.; Rudigier, M.; et al. *γ–γ fast timing with high-performance LaBr$_3$(Ce) scintillators. Prog. Part. Nucl. Phys.* **2024**, *141*, 104152. doi:10.1016/j.ppnp.2024.104152.
111. Tonev, D.; et al. *Transition probabilities in ^{31}P and ^{31}S: A test for isospin symmetry. Phys. Lett. B* **2021**, *821*, 136603. doi:10.1016/j.physletb.2021.136603.
112. Androić, D.; Armstrong, D.S.; Asaturyan, A.; Averett, T.; Balewski, J.; Beaufait, J.; et al. (Q(weak) Collaboration). *First determination of the weak charge of the proton. Phys. Rev. Lett.* **2013**, *111*, 141803. doi:10.1103/PhysRevLett.111.141803.
113. Adhikari, D.; et al. (PREX Collaboration). *Accurate determination of the neutron skin thickness of ^{208}Pb through parity-violation in electron scattering. Phys. Rev. Lett.* **2021**, *126*, 172502. doi:10.1103/PhysRevLett.126.172502.
114. Adhikari, D.; et al. (CREX Collaboration). *Precision determination of the neutral weak form factor of ^{48}Ca. Phys. Rev. Lett.* **2022**, *129*, 042501. doi:10.1103/PhysRevLett.129.042501.
115. Abrahamyan, S.; Ahmed, Z.; Albataineh, H.; et al. (PREX Collaboration). *Measurement of the Neutron Radius of ^{208}Pb through Parity Violation in Electron Scattering. Phys. Rev. Lett.* **2012**, *108*, 112502. doi:10.1103/PhysRevLett.108.112502.
116. Yüksel, E.; Paar, N. *Implications of Parity-Violating Electron Scattering Experiments on ^{48}Ca (CREX) and ^{208}Pb (PREX-II) for Nuclear Energy Density Functionals. Phys. Lett. B* **2023**, *836*, 137622. doi:10.1016/j.physletb.2022.137622.
117. Litvinov, Y.A.; Bishop, S.; Blaum, K.; Bosch, F.; Brandau, C.; Chen, L.X.; et al. *Nuclear physics experiments with ion storage rings. Nucl. Instrum. Methods Phys. Res. B* **2013**, *317*, 603–616. doi:10.1016/j.nimb.2013.07.025.
118. Steck, M.; Litvinov, Y.A. *Heavy-ion storage rings and their use in precision experiments with highly charged ions. Prog. Part. Nucl. Phys.* **2020**, *115*, 103811. doi:10.1016/j.ppnp.2020.103811.
119. Wang, M.; Zhang, M.; Zhou, X.H.; Zhang, Y.H.; Litvinov, Yu.A.; Xu, H.S.; et al. *Bρ-defined isochronous mass spectrometry: An approach for high-precision mass measurements of short-lived nuclei. Phys. Rev. C* **2022**, *106*, L051301. doi:10.1103/PhysRevC.106.L051301.
120. Gade, A.; Glasmacher, T. *In-beam nuclear spectroscopy of bound states with fast exotic ion beams. Prog. Part. Nucl. Phys.* **2008**, *60*, 161–224. doi:10.1016/j.ppnp.2007.08.001.
121. Alder, K.; Winther, A. *Electromagnetic Excitation: Theory of Coulomb Excitation with Heavy Ions*; North-Holland: Amsterdam, The Netherlands, 1975.

© 2025 by the author(s). Distributed under a Creative Commons CC BY license.

Preprints.org (www.preprints.org) | NOT PEER-REVIEWED | Posted: 19 January 2026 doi:10.20944/preprints202601.1421.v1

122. Blaich, T.; et al. *A large area detector for high-energy neutrons (LAND). Nucl. Instrum. Methods Phys. Res. A* **1992**, *314*, 136–154. doi:10.1016/0168-9002(92)90507-Z.
123. Baumann, T.; et al. *The Modular Neutron Array (MoNA).* In *Proceedings of the 4th International Conference on Exotic Nuclei and Atomic Masses (ENAM 2001); AIP Conf. Proc.* **2003**, *680*, 993–996. doi:10.1063/1.1619778.
124. Luther, B.; et al. *MoNA—The Modular Neutron Array at the NSCL. Nucl. Instrum. Methods Phys. Res. A* **2003**, *505*, 33–40. doi:10.1016/S0168-9002(03)01014-3.
125. Nakamura, T.; Kondo, Y. *Large acceptance spectrometers for invariant mass spectroscopy of exotic nuclei and future developments. Nucl. Instrum. Methods Phys. Res. B* **2016**, *376*, 156–161. doi:10.1016/j.nimb.2016.01.003.
126. Lunney, D.; Pearson, J.M.; Thibault, C. *Recent Trends in the Determination of Nuclear Masses. Rev. Mod. Phys.* **2003**, *75*, 1021–1082. doi:10.1103/RevModPhys.75.1021.
127. Kluge, H.-J. *Penning trap mass spectrometry of radionuclides. Int. J. Mass Spectrom.* **2013**, *349–350*, 26–37. doi:10.1016/j.ijms.2013.04.017.
128. Bosch, F.; Litvinov, Yu.A.; Stöhlker, T. *Nuclear physics with unstable ions at storage rings. Prog. Part. Nucl. Phys.* **2013**, *73*, 84–140. doi:10.1016/j.ppnp.2013.07.002.
129. Tu, X.L.; Wang, M.; Litvinov, Yu.A.; et al. *Precision isochronous mass measurements at the storage ring CSRe in Lanzhou. Nucl. Instrum. Methods Phys. Res. A* **2011**, *654*, 213–218. doi:10.1016/j.nima.2011.07.018.
130. Ayyad, Y.; Bazin, D.; Beceiro-Novo, S.; Cortesi, M.; Mittig, W. *Physics and technology of time projection chambers as active targets. Eur. Phys. J. A* **2018**, *54*, 181. doi:10.1140/epja/i2018-12557-7.
131. Bazin, D.; Ahn, T.; Ayyad, Y.; et al. *Low energy nuclear physics with active targets and time projection chambers. Prog. Part. Nucl. Phys.* **2020**, *114*, 103790. doi:10.1016/j.ppnp.2020.103790.
132. Boehnlein, A.; Diefenthaler, M.; Sato, N.; Schram, M.; Ziegler, V.; Fanelli, C.; Hjorth-Jensen, M.; Horn, T.; Kuchera, M.P.; et al. *Colloquium: Machine learning in nuclear physics. Rev. Mod. Phys.* **2022**, *94*, 031003. doi:10.1103/RevModPhys.94.031003.
133. Danielewicz, P.; Lee, J. *Symmetry energy II: Isobaric analog states. Nucl. Phys. A* **2014**, *922*, 1–70. doi:10.1016/j.nuclphysa.2013.11.005.
134. Lattimer, J.M.; Lim, Y. *Constraining the symmetry parameters of the nuclear interaction. Astrophys. J.* **2013**, *771*, 51. doi:10.1088/0004-637X/771/1/51.
135. Somasundaram, R.; Drischler, C.; Tews, I.; Margueron, J. *Constraints on the nuclear symmetry energy from asymmetric-matter calculations. Phys. Rev. C* **2021**, *103*, 045803. doi:10.1103/PhysRevC.103.045803.
136. Liu, Z.W.; Qian, Z.; Xing, R.Y.; Niu, J.R.; Sun, B.Y. *Nuclear fourth-order symmetry energy and its effects on neutron star properties in the relativistic Hartree-Fock theory. Phys. Rev. C* **2018**, *97*, 025801. doi:10.1103/PhysRevC.97.025801.
137. Typel, S.; Brown, B.A. *Neutron radii and the neutron equation of state in relativistic models. Phys. Rev. C* **2001**, *64*, 027302. doi:10.1103/PhysRevC.64.027302.
138. Chen, L.-W.; Ko, C.M.; Li, B.-A. *Nuclear matter symmetry energy and the neutron skin thickness of heavy nuclei. Phys. Rev. C* **2005**, *72*, 064309. doi:10.1103/PhysRevC.72.064309.
139. Lynch, W.G.; Tsang, M.B. *Decoding the density dependence of the nuclear symmetry energy. Phys. Lett. B* **2022**, *830*, 137098. doi:10.1016/j.physletb.2022.137098.
140. Cozma, M.D. *Constraining the density dependence of the symmetry energy using the multiplicity and average p_T ratios of charged pions. Phys. Rev. C* **2017**, *95*, 014601. doi:10.1103/PhysRevC.95.014601.
141. Tsang, M.B.; Friedman, W.A.; Gelbke, C.K.; Lynch, W.G.; Verde, G.; Xu, H.S. *Isotopic scaling in nuclear reactions. Phys. Rev. Lett.* **2001**, *86*, 5023–5026. doi:10.1103/PhysRevLett.86.5023.
142. Demorest, P.B.; Pennucci, T.; Ransom, S.M.; Roberts, M.S.E.; Hessels, J.W.T. *A two-solar-mass neutron star measured using Shapiro delay. Nature* **2010**, *467*, 1081–1083. doi:10.1038/nature09466.
143. Antoniadis, J.; Freire, P.C.C.; Wex, N.; Tauris, T.M.; Lynch, R.S.; van Kerkwijk, M.H.; Kramer, M.; Bassa, C.; Dhillon, V.S.; Driebe, T.; et al. *A massive pulsar in a compact relativistic binary. Science* **2013**, *340*, 448. doi:10.1126/science.1233232.
144. Abbott, B.P.; Abbott, R.; Abbott, T.D.; et al. (LIGO Scientific Collaboration and Virgo Collaboration). *GW170817: Measurements of Neutron Star Radii and Equation of State. Phys. Rev. Lett.* **2018**, *121*, 161101. doi:10.1103/PhysRevLett.121.161101.
145. Isaev, T.A.; Berger, R. *Polyatomic Candidates for Cooling of Molecules with Lasers from Simple Theoretical Concepts. Phys. Rev. Lett.* **2016**, *116*, 063006. doi:10.1103/PhysRevLett.116.063006.
146. Abel, C.; Afach, S.; Ayres, N.J.; Baker, C.A.; Ban, G.; Bison, G.; Bodek, K.; Bondar, V.; Burghoff, M.; et al. *Measurement of the permanent electric dipole moment of the neutron. Phys. Rev. Lett.* **2020**, *124*, 081803. doi:10.1103/PhysRevLett.124.081803.

© 2025 by the author(s). Distributed under a Creative Commons CC BY license.

Preprints.org (www.preprints.org) | NOT PEER-REVIEWED | Posted: 19 January 2026 doi:10.20944/preprints202601.1421.v1

147. Roberts, B.M.; Dzuba, V.A.; Flambaum, V.V. *Parity and time-reversal violation in atomic systems. Annu. Rev. Nucl. Part. Sci.* **2015**, *65*, 63–86. doi:10.1146/annurev-nucl-102014-022331.
148. Dolinski, M.J.; Poon, A.W.P.; Rodejohann, W. *Neutrinoless double-beta decay: Status and prospects. Annu. Rev. Nucl. Part. Sci.* **2019**, *69*, 219–251. doi:10.1146/annurev-nucl-101918-023407.
149. Engel, J.; Menéndez, J. *Status and future of nuclear matrix elements for neutrinoless double-beta decay: A review. Rep. Prog. Phys.* **2017**, *80*, 046301. doi:10.1088/1361-6633/aa5bc5.
150. Flambaum, V.V.; DeMille, D.; Kozlov, M.G. *Time-reversal symmetry violation in molecules induced by nuclear magnetic quadrupole moments. Phys. Rev. Lett.* **2014**, *113*, 103003. doi:10.1103/PhysRevLett.113.103003.
151. Spevak, V.; Auerbach, N.; Flambaum, V.V. *Enhanced T-odd, P-odd electromagnetic moments in reflection asymmetric nuclei. Phys. Rev. C* **1997**, *56*, 1357–1369. doi:10.1103/PhysRevC.56.1357.
152. Dobaczewski, J.; Engel, J. *Nuclear time-reversal violation and the Schiff moment of* ^{225}*Ra. Phys. Rev. Lett.* **2005**, *94*, 232502. doi:10.1103/PhysRevLett.94.232502.
153. Butler, P.A.; Nazarewicz, W. *Intrinsic reflection asymmetry in atomic nuclei. Rev. Mod. Phys.* **1996**, *68*, 349–421. doi:10.1103/RevModPhys.68.349.
154. Parker, R.H.; Dietrich, M.R.; Kalita, M.R.; Lemke, N.D.; Bailey, K.G.; Bishof, M.N.; Greene, J.P.; Holt, R.J.; Korsch, W.; Lu, Z.-T.; Mueller, P.; O'Connor, T.P.; Singh, J.T.; et al. *First measurement of the atomic electric dipole moment of* ^{225}*Ra. Phys. Rev. Lett.* **2015**, *114*, 233002. doi:10.1103/PhysRevLett.114.233002.
155. Dobaczewski, J.; Engel, J.; Kortelainen, M.; Becker, P. *Correlating Schiff moments in the light actinides with octupole moments. Phys. Rev. Lett.* **2018**, *121*, 232501. doi:10.1103/PhysRevLett.121.232501.
156. Gómez-Cadenas, J.J.; Martín-Albo, J.; Menéndez, J.; Mezzetto, M.; Monrabal, F.; Sorel, M. *The search for neutrinoless double-beta decay. La Rivista del Nuovo Cimento* **2023**, *46*, 619–692. doi:10.1007/s40766-023-00049-2.
157. Schechter, J.; Valle, J.W.F. *Neutrinoless double-β decay in $SU(2)\times U(1)$ theories. Phys. Rev. D* **1982**, *25*, 2951–2954. doi:10.1103/PhysRevD.25.2951.
158. Burlac, N.; et al. (LEGEND Collaboration). *Early results of the LEGEND-200 experiment. Nucl. Instrum. Methods Phys. Res. A* **2025**, *1080*, 170779. doi:10.1016/j.nima.2025.170779.
159. Gando, A.; et al. (KamLAND-Zen Collaboration). *KamLAND-Zen 800. Proc. Sci.* **2022**, *ICHEP2022*, 583. doi:10.22323/1.414.0583.
160. Abgrall, N.; et al. (LEGEND Collaboration). LEGEND-1000 Preconceptual Design Report. *arXiv* **2021**, arXiv:2107.11462. doi:10.48550/arXiv.2107.11462.
161. Adhikari, G.; et al. (nEXO Collaboration). *nEXO: Neutrinoless Double Beta Decay Search Beyond* 10^{28} *Year Half-Life Sensitivity. J. Phys. G: Nucl. Part. Phys.* **2022**, *49*, 015104. doi:10.1088/1361-6471/ac3631.
162. Musolf, M.J.; Donnelly, T.W.; Dubach, J.; Pollock, S.J.; et al. *Intermediate-energy semileptonic probes of the hadronic neutral current. Phys. Rep.* **1994**, *239*, 1–178. doi:10.1016/0370-1573(94)90040-X.
163. Beck, D.H.; McKeown, R.D. *Parity-violating electron scattering and nucleon structure. Annu. Rev. Nucl. Part. Sci.* **2001**, *51*, 189–217. doi:10.1146/annurev.nucl.51.101701.132312.
164. Kumar, K.S.; Mantry, S.; Marciano, W.J.; Souder, P.A. *Low-energy measurements of the weak mixing angle. Annu. Rev. Nucl. Part. Sci.* **2013**, *63*, 237–267. doi:10.1146/annurev-nucl-102212-170556.
165. Ahmadi, M.; Alves, B.X.R.; Baker, C.J.; et al. (ALPHA Collaboration). *Observation of the hyperfine spectrum of antihydrogen. Nature* **2017**, *548*, 66–69. doi:10.1038/nature23446.
166. Ahmadi, M.; Alves, B.X.R.; Baker, C.J.; et al. (ALPHA Collaboration). *Characterization of the 1S–2S transition in antihydrogen. Nature* **2018**, *557*, 71–75. doi:10.1038/s41586-018-0017-2.
167. Ulmer, S.; Smorra, C.; Mooser, A.; et al. *High-precision comparison of the antiproton-to-proton charge-to-mass ratio. Nature* **2015**, *524*, 196–199. doi:10.1038/nature14861.
168. Smorra, C.; Sellner, S.; Borchert, M.J.; et al. *A parts-per-billion measurement of the antiproton magnetic moment. Nature* **2017**, *550*, 371–374. doi:10.1038/nature24048.
169. Andreev, V.; Ang, D.G.; DeMille, D.; et al. (ACME Collaboration). *Improved limit on the electric dipole moment of the electron. Nature* **2018**, *562*, 355–360. doi:10.1038/s41586-018-0599-8.
170. Cairncross, W.B.; Gresh, D.N.; Grau, M.; et al. *Precision measurement of the electron's electric dipole moment using trapped molecular ions. Phys. Rev. Lett.* **2017**, *119*, 153001. doi:10.1103/PhysRevLett.119.153001.
171. Isaev, T.A.; Hoekstra, S.; Berger, R. *Laser-cooled RaF as a promising candidate to measure molecular parity violation. Phys. Rev. A* **2010**, *82*, 052521. doi:10.1103/PhysRevA.82.052521.

Disclaimer/Publisher's Note: The statements, opinions and data contained in all publications are solely those of the individual author(s) and contributor(s) and not of MDPI and/or the editor(s). MDPI and/or the editor(s)

© 2025 by the author(s). Distributed under a Creative Commons CC BY license.

Preprints.org (www.preprints.org) | NOT PEER-REVIEWED | Posted: 19 January 2026 doi:10.20944/preprints202601.1421.v1

disclaim responsibility for any injury to people or property resulting from any ideas, methods, instructions or products referred to in the content.

© 2025 by the author(s). Distributed under a Creative Commons CC BY license.